Rheological change and degassing during a trachytic Vulcanian eruption at Kilian Volcano, Chaîne des Puys, France

Mathieu Colombier, Thomas Shea, Alain Burgisser, Timothy Druitt, Lucia Gurioli, Dirk Müller, Francisco Cáceres, Kai-Uwe Hess, Pierre Boivin, Didier Miallier, et al.

Rheological change and degassing during a trachytic Vulcanian eruption at Kilian Volcano, Chaîne des Puys, France

Mathieu Colombier[1]; Thomas Shea[2]; Alain Burgisser[3]; Timothy H. Druitt[4]; Lucia Gurioli[4]; Dirk Müller[1]; Francisco Cáceres[1]; Kai-Uwe Hess[1]; Pierre Boivin[4]; Didier Miallier[5]; and Donald B. Dingwell[1]

[1]Department of Earth and Environmental Sciences, Ludwig-Maximilians-Universität München, Germany; [2]Geology and Geophysics, University of Hawai'i at Mānoa, Honolulu, Hawaii, USA; [3]Univ. Savoie Mont Blanc, CNRS, IRD, ISTerre, F-73376 Le Bourget du Lac, France; [4]Université Clermont Auvergne -CNRS-IRD, OPGC, Laboratoire Magmas et Volcans, F-63100, Clermont-Ferrand, France; [5] Université Clermont Auvergne, CNRS–IN2P3, LPC, F-63000 Clermont-Ferrand, France

Keywords: Effusive-explosive transitions, Trachytic magma, Vulcanian eruption, Viscosity, Crystallization, Degassing, Nanolites, Cristobalite.

Abstract

Magma ascent during silicic dome-forming eruptions is characterized by significant changes in magma viscosity, permeability and gas overpressure in the conduit. These changes depend on a set of parameters such as ascent rate, outgassing and crystallization efficiency, and magma viscosity which in turn may influence the prevailing conditions for effusive versus explosive activity. Here, we combine chemical and textural analyses of tephra with viscosity models to provide a better understanding of the effusive-explosive transitions during Vulcanian phases of the 9.4 ka eruption of Kilian Volcano, Chaîne des Puys, France. Our results suggest that effusive activity at the onset of Vulcanian episodes at Kilian Volcano was promoted by (i) rapid ascent of initially crystal-poor and volatile-rich trachytic magma, (ii) a substantial bulk and melt viscosity increase driven by extensive volatile loss and crystallization, and (iii) efficient degassing/outgassing in a crystal-rich magma at shallow depths. Trachytic magma repeatedly replenished the upper conduit, and variations in the amount of decompression and cooling caused vertical textural stratification, leading to variable degrees of crystallization and outgassing. Outgassing promoted effusive dome growth and occurred via gas percolation through large interconnected vesicles, fractures and tuffisite veins, fostering the formation of

cristobalite in the carapace and talus regions. Build-up of overpressure was likely caused by closing of pore space (bubbles and fractures) in the dome through a combination of pore collapse, cristobalite formation, sintering in tuffisite veins or limited pre-fragmentation coalescence in the dome or underlying hot vesicular magma. Sealing of the carapace may have caused a transition from open to closed system degassing and to renewed explosive activity. We generalize our findings to propose that the broad spectrum of eruptive styles for trachytic magmas may be inherited from a combination of characteristics of trachytic melts, that include high water solubility and diffusivity, rapid microlite growth, and low melt viscosity compared to their more evolved subalkaline dacitic and rhyolitic equivalents. We show that trachytes may erupt with a similar style (e.g., Vulcanian) but at significantly higher ascent rates than their andesitic, dacitic and rhyolitic counterparts. This suggests that the periodicity of effusive-explosive transitions at trachytic volcanoes may differ from that observed at the well-monitored andesitic, dacitic and rhyolitic volcanoes, which has implications for hazard assessment associated with trachytic eruptions.

Introduction

Understanding and forecasting effusive-explosive transitions during intermediate-to-silicic volcanic eruptions is a key objective of volcanology. Such transitions occur frequently (e.g., Cassidy et al. 2018), yet they remain difficult to anticipate. During andesitic, dacitic and trachytic eruptions, effusive phases commonly lead to the emplacement of crystal-rich lava domes or plugs stalling at shallow levels of the conduit (Platz et al. 2007; Lavallée et al. 2012; Kushnir et al. 2016; Colombier et al. 2017a; Heap et al. 2018). Explosive activity and conduit evacuation can in turn be triggered by the pressurization of underlying vesicular magma which ultimately yields a downward propagation of a fragmentation front within the conduit (e.g., Druitt et al. 2002; Platz et al. 2007; Giachetti et al. 2010; Calder et al. 2015) or by over-pressurization of the dome itself (e.g., Boudon et al. 2015). As a result of these transitions, dense, crystal-rich, dome-derived pyroclasts and highly vesicular, conduit-derived pumice pyroclasts commonly coexist in the deposits of Vulcanian eruptions leading to bimodal porosity/density distributions of the pyroclasts (Formenti and Druitt 2003; Adams et al. 2006; Mujin and Nakamura 2014; Colombier et al. 2017a). Crystallization during magma ascent, and stagnation at shallow levels, is mostly driven by processes related to decompression, degassing and/or cooling (e.g., Blundy and Cashman 2001; Arzilli and Caroll 2013; Zorn et al. 2018).

Effusive-explosive transitions have been proposed to arise from differences in magma ascent rate (e.g., Platz et al. 2007; Cassidy et al. 2018), degassing conditions (e.g., Eichelberger et al. 1986; Jaupart and Allègre 1991), pre- or syn-eruptive volatile content (e.g., Andujar and Scaillet 2012; Forte and Castro 2019), rheological changes in the magma (e.g., Moitra et al. 2018; Cassidy et al. 2018) and lava-water interaction (e.g., Belousov et al. 2011; Fitch et al. 2017). The emplacement of lava domes is typically associated with significant gas loss from the magma by outgassing through connected bubble networks, fractures or intergranular pore space (Kendrick et al. 2016; Colombier et al. 2017b; Lamur et al. 2017; Yoshimura et al. 2019). Magma permeability is the dominant factor controlling the ability of gas to escape from the magma, and its evolution is both complex and highly transient in lava domes (e.g., Mueller et al. 2005). Rheological changes in the lava dome also have an important role in controlling cyclic and hybrid eruptive style (e.g., Lavallée et al. 2013). They are principally governed by the kinetics of crystallization, bubble nucleation and growth, and variations in volatile content and temperature (cooling or heating). All these processes may have competing effects on eruptive style. As an example, an increase in magma viscosity may (1) lead to a slower ascent rate, which in turn may promote gas escape, magma cooling and effusive activity, or (2) have the adverse effect of causing gas overpressure and magma brittle fragmentation, leading to explosive eruption. Finally, ascent rate controls the time available for the formation of a permeable magma. Faster ascent rates offer less time for permeable gas pathways to develop, thereby favouring explosive activity (Cassidy et al. 2018).

Trachytic (and phonolitic) silicate melts differ strongly from their more widespread, subalkaline counterparts (andesites, dacites and rhyolites) in several ways. Firstly, they have lower viscosities at similar conditions of SiO_2 content, temperatures and dissolved H_2O than rhyolitic melts due to differences in melt compositions (e.g., Andujar and Scaillet 2012). Secondly, trachytic melts are inferred to crystallize faster than subalkaline compositions, with higher crystal nucleation and growth rates leading to higher crystallinities and crystal number densities on a given timescale (Arzilli and Caroll 2013; Shea et al. 2017). As crystals are known to promote permeable gas escape at lower porosities (e.g., Blower 2001; Oppenheimer et al. 2015; Colombier et al. 2017b; Lindoo et al. 2017; Colombier et al. 2020), one might expect that the timing and efficiency of outgassing are strongly influenced by the high rates of crystallization experienced by trachytic magmas during ascent. Such rapid crystallization may also promote heterogenous bubble nucleation on crystals (Cluzel et al. 2008) thereby reducing volatile supersaturation pressure and promoting earlier degassing in the conduit. Additionally, water solubility is higher in trachytic melts than in rhyolites, with water contents exceeding 7

wt.% at ~200MPa (Di Matteo et al. 2004; Martel et al. 2013). Depending on the ascent rates of trachytic magmas, and the diffusivity of dissolved water, this high water solubility may lead to preservation of high water contents even close to the surface (Di Matteo et al. 2004). On the other hand, slow ascent and high water diffusivity allow magmas to track near-equilibrium water solubility which is very low at shallow depths (Di Matteo et al. 2004). Fanara et al (2013) predicted high water diffusivities and therefore more efficient degassing in trachytic melts than in their rhyolitic counterparts at high temperature and high pressures.

In this paper we combine textural and chemical analysis of pyroclasts from the 9.4 ka trachytic Vulcanian eruption of Kilian Volcano (Colombier et al. 2017a) in order to unravel the mechanisms responsible for effusive-explosive transition. This volcano is located in the Chaîne des Puys, a dormant magmatic system approximately 6 km east from the city of Clermont-Ferrand – a proximity which brings with it some concerns regarding volcanic hazards and risk (Delcamp et al. 2014; Latutrie et al. 2016). Constraining the eruptive style of Kilian Volcano is not only a key to unlocking the characteristics of one of the dominant types of volcanism at the Chaîne des Puys (Martel et al. 2013), but also to improve our understanding of eruptive processes and hazards at monogenetic volcanoes worldwide. More generally, a better understanding of the dynamics behind effusive-explosive transitions is of primary importance to better assess hazards related to cyclic dome-forming eruptions. Although they are less ubiquitous, and commonly less voluminous, than subalkaline magmas, trachytic magmas are often associated with violent explosive volcanic activity (Rosi et al. 1999) and some trachytic volcanoes are located close to highly populated areas (e.g., Campi Flegrei, Italy). Studying the chemical and textural characteristics of products from past trachytic eruptions is essential to identify their eruptive style controls, and to shed light on how they differ from andesitic-rhyolitic magmas.

We propose in what follows that the specific characteristics of trachytic melts such as water solubility, water diffusivity, viscosity and crystal growth kinetics were likely responsible for rapid changes in magma rheology during the 9.4 ka Kilian eruption and that these rheological changes, coupled with a high outgassing efficiency exerted a primary control on the kinetics of effusive-explosive transitions at Kilian Volcano. We illustrate how our findings can be extrapolated to other trachytic volcanoes, and show that the degree of crystallization, viscosity and efficiency of degassing/outgassing are key parameters regulating the eruptive style and cyclicity of trachytic eruptions.

Geological setting

Kilian Volcano is one of several trachytic monogenetic edifices belonging to the Chaîne des Puys, France (Fig. 1). It consists of a crater (enlarged by quarrying) and the partial remains of a lava dome. The Kilian eruption occurred 9.4 ka ago (Miallier et al. 2012) and was characterized by a succession of five eruptive episodes ranging from Vulcanian (dome- or plug-forming) to sub-Plinian (dome- or plug-free) activity, possibly preceded by a phreatic opening phase (Boivin et al. 2017; Colombier et al. 2017a). The reader is referred to Colombier et al. (2017a) for a detailed description of the stratigraphy and related eruptive sequence. Here, we focus on the Vulcanian episodes that have been recently interpreted to result from overpressurization of the hot, vesicular magma column below an outgassed, crystal-rich plug or dome (Colombier et al. 2017a). Despite their different bulk chemical compositions, these Vulcanian explosions and their products shared several similarities with Vulcanian activity at Soufrière Hills volcano in Montserrat (Formenti and Druitt 2003; Giachetti et al. 2010; Colombier et al. 2017a).

Proximal tephra deposits from the eruption cover a large part of the Chaîne des Puys, including the top and northern flank of the Puy de Dôme edifice (1450 m a.s.l) located 800 m north-east of Kilian crater (Colombier et al. 2017a; Boivin and Thouret 2014; Portal et al. 2019). A distal tephra layer possibly from Kilian has been identified as far as Soppensee lake in Switzerland (Lane et al. 2011). Van Wyk de Vries et al (2014) suggested that Kilian crater was created by explosive activity due to the presence of a shallow magmatic intrusion (i.e. cryptodome) on the bulged edifice of Puy Grosmanaux to the south. Kilian crater is partially filled by the remains of a 200-m-wide, 50 to 100 m thick, trachytic lava dome that creates a positive gravity anomaly (Portal et al. 2016; Boivin et al. 2017). This dome was probably emplaced following the explosive phases.

The samples analyzed in this study are derived from three Vulcanian episodes at Kilian Volcano (Colombier et al. 2017a) and were mainly sampled at the Coupe des Muletiers outcrop located approximately 500 m NE of Kilian crater (Fig. 1). A few additional samples were taken from deposits on the summit of Puy de Dôme volcano and one *in situ* dome rock was sampled from the exterior of the dome remnants in Kilian crater (Fig. 1). We note that an additional type of massive trachyte is also associated to Kilian dome although it is not cropping out in Kilian crater (Boivin et al. 2015). This lithology has been widely quarried and used for building and ornamental purposes at the Gallo-Roman period and is no longer visible in the crater because it has been covered by quarrying waste and colluvial (Boivin et al. 2015). This peculiar type of

trachyte will not be discussed in this study as it is also absent from the tephra deposits and likely represents a late effusive stage.

Methods

Textural, petro-physical and chemical analysis

Textural observations were made on scanning electron microscope using back-scattered electron images taken on a HITACHI SU 5000 Schottky FE-SEM and electron microprobes at the Ludwig Maximilian University of Munich and at the University of Hawai'i at Mānoa.

We analyzed the compositions of interstitial glass and microlites in two pumice pyroclasts and six dome pyroclasts using Electron Probe Micro-analysis to complement and complete the preliminary dataset of Colombier et al (2017a). Glassy areas in some dome pyroclasts were too small to be analyzed. Microprobe analyses at the Ludwig Maximilian University were carried out with a Cameca SX-100 instrument. A 10 µm defocused beam at an accelerating voltage of 15 keV and a current of 5 nA was used in glass analysis in order to limit Na loss. Calibration was done on the following standards: wollastonite (Ca); albite (Na, Si); periclase (Mg); orthoclase (K, Al); Fe_2O_3 (Fe); Cr_2O_3 (Cr); ilmenite (Ti); bustamite (Mn); apatite (P); vanadinite (Cl); anhydrite (S). Peak counting time was 10s for each element (5s for background on each side of the peak). For matrix correction the PAP routine, implemented in the Cameca PeakSight software, was used. Another set of analyses was conducted at the University of Hawai'i at Mānoa using a JEOL Field-emission Hyperprobe JXA-8500 device, with an accelerating voltage of 15kV and a 10nA beam current. Standards used were: VG2 and STG56 glasses (Si, Al, Fe, Ca), Sphene glass (Ti), Verma garnet (Mn), Springwater olivine (Mg), Orthoclase (K), Amelia albite (Na), Durango apatite (Cl, P). On-peak count times were 20s (Si, Ti, Na, Fe, K, P, Mn), 30s (Ca), and 60s (Cl, Al) with half of those count times off-peak for background measurement. The time-dependent intensity correction implemented in the software Probe for EPMA© was used to track and correct for Na loss and Si gains when needed. Analytical precision was better than 1% relative for Si, Al, Mg, Fe, Ca, 3% relative for Na, K, Ti, 10% relative for P and Cl. Due to the age of the deposits, secondary rehydration by meteoric water caused totals to be lower than 100%. As a result, glasses were normalized to 100% to allow comparison between different pyroclasts but uncorrected raw data are available in Supplementary material. Interlaboratory microprobe analysis was carried for practical reasons, and chemical analysis of the same pyroclast measured at the Ludwig Maximilian

University of Munich and at the University of Hawai‘i at Mānoa yielded similar results. We also performed additional textural analyses and chemical mapping of an *in situ* dome rock at the scanning electron microscope at the Laboratoire Magmas et Volcans of Clermont-Ferrand.

Eight pumice pyroclasts and five dome pyroclasts were selected for X-ray diffraction (XRD). The finely ground samples were mixed with ~17 wt.% of silicon (Alfa Aesar Silicon powder, 99.5 % purity) as internal standard for quantitative Rietveld refinement. For Rietveld refinement the software *Profex 3.10.2* (Döbelin et al. 2015) was used. Measurements were performed with a GE X-ray diffractometer (XRD 3003 TT) in Bragg-Brentano geometry in a 2 theta-range of 10 - 100 ° by using Cu K_{a1} radiation.

X-ray fluorescence whole rock analyses were carried out on 7 pumice pyroclasts and 4 dome pyroclasts at the Institute of Geosciences, Johannes Gutenberg University Mainz, Germany, using a Philips MagiXPRO device. Loss on ignition was determined after heating the sample for 2 h at 980 °C. The major elements were measured on glass beads, prepared from a mixture of 0.4 g sample powder and 5.2 g $Li_2B_4O_7$.

Simultaneous thermal analysis

Two pumice pyroclasts and one dome pyroclast were heated in a STA Netzsch 404C at a heating rate of 10° $C.min^{-1}$ up to 1000°C to retrieve the glass transition temperature (T_g) and to distinguish between the meteoric and magmatic water contents using thermogravimetric measurement of the mass loss during heating.

These results have been combined with porosity, permeability, crystallinity, whole rock and glass analyses and textural data from our previous study (Table 1; Colombier et al. 2017a).

Results

Classification of pyroclasts based on textural observations

In this study we mainly focus on pyroclasts from the initial and final Vulcanian phases of the Kilian eruption and include one pyroclast from intermediate sub-Plinian phases (units U1, K1 and K2 in figure 3 from Colombier et al. 2017a). For simplicity, we use the same classification as in Colombier et al. (2017a) to distinguish pumice (>40% porosity) from dense dome-derived pyroclasts (<40% porosity; hereafter referred to as dome pyroclasts). In reality, there is an overlap in the porosity range of the two populations. The juvenile pyroclasts analyzed are mostly lapilli in the grain size fraction 16-32 mm, with a few larger lapilli of the fraction 32-64 mm (Table 1).

Pumice pyroclasts are beige-gray in color and range from highly rounded to highly angular in shape (Fig. 2a, c and d) which may reflect (i) a mixed mode of tephra emplacement between PDC and fallout, with more abrasion and rounding for the PDC pyroclasts (Colombier et al. 2017a) or (ii) different degree of rounding due to variable porosities in this population. Rare breadcrust textures have been observed in a few, dense pumice lapilli and bombs. On the other hand, dome pyroclasts are gray to dark-gray and are essentially angular, with only a few sub-rounded particles (Fig. 2b). Some of these pyroclasts show breadcrust textures (Fig. 2e) and banded pyroclasts are ubiquitous in this population (Fig. 2f).

Pumice pyroclasts contain near-spherical to deformed vesicles (Fig. 3a-d). The degree of deformation of the vesicles seems to intensify with decreasing porosity and increasing crystallinity (Fig. 3a-d).

The range of textures in the dome pyroclasts population is highly variable between pyroclasts of similar porosity. We identify three main populations of dome pyroclasts: (i) a Type 1 consisting of dome pyroclasts with small isolated vesicles and larger coalesced vesicles organized in clusters within interstitial glassy areas between microlites (crystallinity is lower than in Type 2 pyroclasts; Fig. 3e-g); (ii) a Type 2 population with pyroclasts characterized by diktytaxitic textures with a high number density of small interconnected vesicles in a nearly holocrystalline matrix, and by the presence of cristobalite in interconnected vesicle clusters (Fig. 3h-j); (iii) a Type 3 population including brecciated dome pyroclasts with banded and sheared textural layers alternating with more brecciated domains consisting of granular patches with variable degree of sintering (Fig. 3k, l). The banded areas contain large phenocrysts of feldspar, kaersutite, biotite and occasionally, cristobalite, and ash particles and the grain size is highly variable.

Networks of pyroclast-wide cracks are present in all dome pyroclasts but are more developed in the Type 2 and 3 populations. We also observed locally interconnected vesicle chains in pumice and dome pyroclasts (Fig. 4a, b). These different textural lithologies are present in all the deposits associated with Vulcanian episodes of the Kilian eruption (Colombier et al. 2017a).

Finally, the *in situ* dome rock sample coming from the external part of dome remnants outcropping in Kilian crater show textures similar to that of the Type 2 dome pyroclasts from the deposits. Similarities include the diktytaxitic texture with a holocrystalline matrix and absence of glass, and the presence of cristobalite in the interconnected vesicles clusters highlighted by chemical mapping (Fig. 4f, g).

Chemical analysis and crystallinity

All the pyroclasts are trachytic in bulk rock composition (Fig. 5; Table SM1). No bulk rock oxide concentrations correlate with pyroclast type except for SiO_2, which is slightly higher in the Type 2 dome pyroclasts than in the Type 1 and Type 3 dome pyroclasts and pumice pyroclasts due to the presence of cristobalite (Table SM1). Glass compositions evolve from dominantly trachytic in the pumice pyroclasts to dominantly rhyolitic in the dome pyroclasts (Fig. 5; Table SM1).

The principal phenocrysts identified by microprobe are oligoclase and anorthoclase with minor amounts of kaersutite, magnetite, ilmenite, apatite, cristobalite and zircon. The samples analyzed here lack phenocrysts of clinopyroxene although previous studies noted the presence of rare clinopyroxene in Kilian Tephra (Juvigné et al. 1992; Martel et al. 2013). The microlites are essentially oligoclase to anorthoclase feldspars (Fig. 5), and Fe-Ti oxides. Oxide nanolites (<1µm) are also abundant in Type 1 and 2 dome pyroclasts and frequently decorate feldspar microlites (Fig. 4d, e; Colombier et al. 2017a). We note that rare submicron nano-crystals were also occasionally observed in pumice pyroclasts. The number density of Fe-Ti oxide nanolites and microlites is considerably higher in dome pyroclasts than in pumice pyroclasts, as reported for other Vulcanian eruptions (e.g., Mujin and Nakamura 2014).

XRD analysis yields the identity and quantity of crystalline phases in the pyroclasts (Fig. 6a; Table 2). Phase proportions in wt % were converted to volume fractions using the known densities of the glass and crystalline phases. Although Fe-Ti oxide microlites and nanolites are

ubiquitous in these samples and have a high number density (Colombier et al. 2017a), they were not detected by XRD implying that Fe-Ti oxides represent each less than 2 wt% (XRD detection limit) in all pyroclasts. The crystallinity estimated from XRD ranges from 50 to 94 vol% (Table 2). The most abundant phases are oligoclase and anorthoclase (50–87 vol%). Kaersutite is found only in one Type 1 dome pyroclast (2.2 vol%) and cristobalite appears mostly in the Type 2 dome pyroclasts (~6.5 vol%), and in smaller amount in one Type 1 dome pyroclast only (~4 vol%; Table 2).

Porosity distributions (Colombier et al. 2017a) are bimodal, with pumice and dome pyroclast populations centered around ~60% and 25% porosities respectively (Fig. 6b). The crystallinity of pyroclasts clearly increases with decreasing porosity (or increasing density) (Fig. 6a). The dome pyroclasts show crystallinities between 68.4 and 93.5 vol% whereas the pumice pyroclasts contain 49.9–66.7 vol% crystals. The crystallinities obtained by XRD and via 2D image analysis (Colombier et al. 2017a) show the same trend of increasing crystallinity with porosity, but values of crystallnity measured using image analysis are systematically 30–40 vol% lower than those obtained with XRD (Fig. 6a). A calibration of the XRD technique for crystallinity quantification showed that the error is less than 5 vol% with this method (Fig. SM3 in the supplementary material), which implies that the discrepancy between XRD and image analysis arises from issues with the latter technique. Limits to contrast in the scanning electron microscope images and the fact that microlites below a certain size cannot be resolved and quantified may be responsible for this apparent discrepancy in crystallinity. Rowe et al (2012) have discussed that two-dimensional imaging techniques are insufficient for characterizing crystallinity in samples where the groundmass does not contain an easily identifiable glassy component, which is the case here for Kilian samples. D'Oriano et al (2005) have pointed out that feldspar composition for trachytic-phonolitic melts is close to that of the residual liquid and that subsequent low grey scale contrast of feldspars and matrix glass on BSE images constitute an obstacle for detailed textural analysis. This discrepancy between XRD and image analysis is likely more significant in highly crystal-rich samples such as Kilian trachytes. Devitrification and the presence of high quantities of small crystals not quantified during image treatment may be an additional cause of discrepancy between crystallinities measured by XRD and image analysis (Rowe et al. 2012; Andrade et al. 2017). Regardless of the method, data obtained by the two techniques show similar features, with Type 1 dome pyroclasts being less crystalline than Type 2 dome pyroclasts (Fig. 6a; Table 1 and 2). Interestingly, the crystallinity increases with decreasing porosity in the pumice population, and the least vesicular pumice has crystallinities approaching some of the Type 1 dome pyroclasts (Fig. 6a; Table 1 and 2). Only

one type 3 banded-pyroclast was measured and showed the lowest crystallinity in the dome population (68.4 vol%).

Glass compositions

The glass compositions of pumice and Type 1 dome clats form a nearly continuous spectrum of increasing SiO_2 and decreasing Al_2O_3 and alkali content, likely associated with extensive feldspar microlite crystallization (Fig. 7). More generally, elements that are compatible in anorthoclase (Al_2O_3, Na_2O, CaO) show trends consistent with extensive feldspar crystallization. By contrast, MgO is incompatible in anorthoclase, yet also decreases with increasing SiO_2. We attribute this decrease to crystallization of kaersutite containing ~10 wt.% MgO on average. Cl is also incompatible in most crystallizing phases (kaersutite contains only up to 0.15 wt.% in these rocks) and should increase in the melt during crystallization. However, Cl slightly decreases with increasing SiO_2 in the interstitial glass between pumice and dome pyroclast, suggesting possible loss to degassing (Fig. 7). The composition of the most vesicular pumice pyroclasts matches closely the composition of melt inclusions trapped in amphiboles and plagioclase phenocrysts (Martel et al. 2013), suggesting little crystallization occurred between the time when inclusions were trapped and the least crystal-rich pumice pyroclasts were erupted. In addition, SiO_2, TiO_2 and Fe_2O_3 are higher in the dome glass (Type 1 and 3) compared to the pumice glass, while MgO, CaO, Na_2O, K_2O, Al_2O_3 and Cl are higher in the pumice glass (Fig. 8). F content in the glass was below the detection limit (500 ppm). The Type 3 dome pyroclasts (banded and brecciated pyroclasts) have a similar range in glass SiO_2 compared to Type 1 dome pyroclasts, but with lower average values for alkalis, TiO_2, Fe_2O_3, MnO and higher values of MgO, Al_2O_3, CaO and P_2O_5 (Fig. 5, 7, 8; Table SM1 in supplementary material). This evolution of glass composition from vesicular pumice to denser dome pyroclasts likely reflects the predominant crystallization of feldspars together with minor amounts of magnetite microlites.

Chemical mapping revealed a zonation in the feldspar microlites in the dome pyroclasts, with large microlites showing more Ca-rich and K-poor cores than rims and smaller microlites (Fig. 4). Therefore, the large variations in K_2O and CaO observed for feldspar composition in figure 7 likely reflect an evolution in time toward higher and lower values of K_2O and CaO, respectively, during feldspar crystallization. This observation agrees with the fact that data for

feldspar phenocrysts formed early in the crystallization process plot towards the CaO-rich and K_2O-poor endmember of the feldspar population (Fig. 7).

Viscosity model

The thermal analysis yielded a glass transition temperature T_g ~ 689°C (Fig. 9). We then estimated the dry and hydrous melt viscosity and magmatic water content of the trachytic magma by combining the viscosity models of Gottsmann et al (2002) and Giordano et al (2004). A detailed description of the procedure is given in the supplementary material. Output of the model yielded a water content of 0.04 wt % and a viscosity of $10^{11.07}$ Pa.s at T_g in the pumice population. The viscosity with this model assuming a similar water content at eruptive temperature of 775°C (Martel et al. 2013) for the pumice population yielded ~$10^{9.38}$ Pa.s. We emphasize that these viscosity estimates represent the values at the time of quenching of the pumice pyroclasts and viscosity may have been significantly lower during fragmentation if the water content was higher. At pre-eruptive storage conditions of 300–400 MPa, ~8 wt% H_2O, and T=775°C (Martel et al. 2013), the Giordano et al (2004) model yields a melt viscosity $10^{1.71}$ Pa.s.

The low modelled magmatic water content in the glass of the pumice pyroclasts at the time of quenching compares nicely with the results of the thermogravimetric analysis (Fig. 9). This analysis shows mass loss only below Tg, suggesting the presence of some meteoric water but no magmatic water in pumice and dome pyroclasts. We note that Cl was likely stabilized in the melt phase during this thermal treatment due to the high iron content preventing volatilization and Cl escape (Dingwell and Hess 1998). Next, we used the Giordano et al (2008) model to calculate the melt viscosity of the Type 1 dome pyroclasts with a rhyolitic glass composition and assuming a water content of 0.02 (lowest solubility for rhyolitic composition). This yielded a viscosity of ~$10^{11.69}$ Pa.s at 775°C.

Origin of the different types of pyroclasts

We hereafter combine information from textural and chemical analysis with viscosity estimations to shed light on the origin of the different types of pyroclasts and on conduit stratigraphy prior to Vulcanian episodes at Kilian Volcano.

386

387 Pumice population

388

389 Glasses within the most vesicular pumice pyroclasts are similar in composition to melt
390 inclusions measured in feldspar and amphibole phenocrysts by Martel et al (2013). This
391 similarity suggests that microlites did not significantly modify the melt composition in the
392 pumice population after phenocryst formation.
393 scanning electron microscope observations and XRD analysis indicate that crystallinity
394 increases with decreasing porosity of the pumice pyroclasts. Furthermore, the crystallinity in
395 the least vesicular pumice pyroclasts approaches values measured in some of the Type 1 dome
396 pyroclasts (Fig. 6a). These pumice pyroclasts were therefore likely emplaced in an intermediate
397 region below the dome, which experienced greater extents of decompression, cooling,
398 degassing and therefore more crystallization than deeper in the conduit. Alternatively, pumice
399 pyroclasts with higher microlite content may originate from the conduit margins where (i) lower
400 temperatures promote crystallization or (ii) preferential, strain-induced degassing (e.g. Shea et
401 al. 2014) may have accelerated degassing-induced crystallization. These transitional zones
402 might explain the overlap in crystallinity and porosity between the pumice and dome
403 populations (Fig. 6).
404 High porosity pumice pyroclasts likely originate from deeper and more central zones of
405 the conduit and experienced significant syn- and post-fragmentation vesiculation and possibly
406 outgassing (e.g. Giachetti et al. 2010; Giachetti et al. 2015). This scenario would be consistent
407 with the low magmatic water content modelled and measured in the pumice pyroclasts.
408 Evidence for post-fragmentation vesiculation is also recorded by the presence of bread-crust
409 textures at the surface of bombs and lapilli (Colombier et al. 2017a).
410

411 Type 1 Dome pyroclasts

412

413 These dome pyroclasts are less crystalline than those of Type 2 but are more crystalline than
414 most of the pumice and Type 3 pyroclasts. The melt composition during magma ascent was
415 initially similar to that of pumice and melt inclusions and subsequently evolved by
416 crystallization of mostly feldspar and minor amounts of kaersutite and magnetite. Measured
417 glass compositions show more heterogenous and depleted Cl contents compared to the pumice

418 population. Depleted and heterogenous Cl contents in volcanic rocks have been reported
419 elsewhere and attributed to (i) leaching or devolatilization of Cl by escaping steam with
420 subsequent degassing to the surface (e.g., Soufrière Hills volcano; Harford et al. 2003; Horwell
421 et al. 2013; Schipper et al. 2019), (ii) outgassing (Yoshimura et al. 2019; Schipper et al. 2019),
422 (iii) devitrification in rhyolitic melts (Schipper et al. 2019) or (iv) groundmass crystallization
423 in a slowly cooling magma (Signorelli and Carroll 2002). The latter process can be ruled out as
424 groundmass crystallization of microlites with low Cl content would have the inverse effect of
425 increasing the Cl content from pumice to dome pyroclasts. We thus propose that permeable gas
426 and fluid transport are likely responsible for the heterogeneous and depleted Cl concentrations
427 in the dome pyroclasts at Kilian. We note that a low Cl content was measured locally in two
428 pumice pyroclasts, indicating that a similar process may also have occurred to a lesser extent
429 and in more localized areas in the pumice population.
430 The presence of networks of large interconnected vesicle clusters and the high
431 permeability (~10^{-12} m²; Table 1) of Type 1 dome pyroclasts indicates that permeable gas escape
432 likely occurred in this population (possibly aided by formation of cracks). Additional
433 permeability measurements would be required to better explore differences between the four
434 pyroclast populations. Cristobalite is generally rare in Type 1 samples but was observed in one
435 pyroclast, with lower concentrations than those found in the Type 2 pyroclasts. The low
436 cristobalite abundance relative to Type 2 pyroclasts in turn suggests more limited or later
437 occurrence of outgassing and fluid transport. A population of small isolated vesicles coexists
438 with the large vesicle clusters, previously attributed to a late stage event of syn-eruptive bubble
439 nucleation and growth event (Colombier et al. 2017a). This late stage of bubble nucleation may
440 have proceeded heterogeneously on feldspar and Fe-Ti microlites (e.g., Shea 2017; Pleše et al.
441 2018). The low connectivity and size of these small bubbles means that this second vesiculation
442 event likely had a small influence on permeability and outgassing compared with macropores.
443 Type 1 pyroclasts can be considered as a gradual transition between pumice pyroclasts
444 and Type 2 rocks in term of textures, composition, crystallinity and the presence and amount
445 of oxide nanolites and cristobalite (Fig. 3, 4 and 6; Table 2). As discussed above, pumice
446 pyroclasts are inferred to represent hot vesicular magma beneath the lava dome. We argue in
447 the next section that the Type 2 pyroclasts likely arise from the upper part of the dome (talus
448 and carapace). We therefore propose that the Type 1 population corresponds to a transitional
449 region in the interior of the dome above the underlying hot and less viscous magma and beneath
450 the diktytaxitic carapace.
451

452 Type 2 Dome pyroclasts

453

454 These pyroclasts display diktytaxitic textures, and are more crystal-rich than the Type 1
455 pyroclasts at a similar porosity with scarce glassy areas only recognized through XRD analyses
456 (Fig. 6). The presence of this texture suggests either (i) more extensive crystallization, (ii) gas-
457 filter pressing that may remove the highly viscous melt from these parts of the dome or (iii)
458 dissolution of the glass through intense leaching.

459 Cristobalite microlites are present within scanning electron microscope and microprobe
460 images in all Type 2 pyroclasts (Fig. 3; Table 1 and 2). Cristobalite is almost systematically
461 located in interconnected macro-pores that resemble the vesicle clusters observed in the Type
462 1 dome pyroclasts but with more irregular shapes due to higher crystallinities and smaller size
463 indicative of more advanced pore collapse (Fig. 3). Thus, cristobalite likely crystallized in the
464 connected porous network of these dome pyroclasts. Cristobalite is frequently found in dome
465 rocks with diktytaxitic textures from other lava domes and lavas such as at Lewotolo volcano,
466 Soufrière Hills volcano in Montserrat, Volcán de Colima, Cordón Caulle, Merapi or Mount
467 Taranaki (e.g., de Hoog et al. 2005; Williamson et al. 2010; Lavallée et al. 2012; Schipper et
468 al. 2015; Kushnir et al. 2016; Preece et al. 2016; Zorn et al. 2018). Cristobalite has also been
469 recognized in other Chaîne des Puys trachytic domes at Chopine and Puy de Dôme volcanoes
470 (Boudon et al. 2015; Deniel et al. 2020). The presence of cristobalite is often taken as an
471 evidence for prolonged residence time in the dome during outgassing (e.g., Kendrick et al.
472 2016) although cristobalite precipitation itself is believed to be a rapid process (typically in the
473 order of few hours; Williamson et al. 2010; Damby et al. 2014). Cristobalite formation has been
474 attributed to gas filter pressing (Kushnir et al. 2016), devitrification (e.g., Horwell et al. 2013;
475 Schipper et al. 2015, 2017) and/or precipitation from silica-rich fluids percolating through the
476 dome (Horwell et al. 2013; Boudon et al. 2015; Kendrick et al. 2016). In our case, the fact that
477 cristobalite is always observed in the connected macro porosity suggests that it was formed by
478 permeable transport of Si-rich fluids during outgassing and possibly hydrothermal activity at
479 shallow levels.

480 The increase in bulk SiO_2 in Type 2 dome pyroclasts (Table SM1) suggests that silica
481 was transported into this region of the dome from external sources outside the magmatic system,
482 as proposed by Horwell et al (2013), or from inner regions of the dome. The presence of
483 cristobalite and diktytaxitic textures are characteristics of external regions of lava domes, and
484 are typically found in the carapace or talus region (Boudon et al. 2015; Kushnir et al. 2016;
485 Heap et al. 2018). We propose that the source of SiO_2 arises from leaching of Si-rich melt areas

from the Type 1 interior region of the dome and subsequent transport to the external carapace or talus region. Leaching may proceed via corrosion through magmatic H_2O and/or acid solutions/vapors such as HF followed by scavenging of alkalis and Si present in the glass and crystalline phases, and subsequent entrainment in Si-rich fluids (Horwell et al. 2013; Schipper et al. 2015). This scenario can therefore be seen as intermediate between a "bulk transport" and a "local redistribution" of silica (Horwell et al. 2013; Schipper et al. 2015) in the case of Kilian with a process in which the vapor source comes from the dome itself (in agreement with local redistribution) but involves some transport and causes change in the bulk SiO2 content (compatible with bulk transport).

This origin in the exterior of the dome is further suggested by the presence and high number density of Fe-Ti oxide nanolites in the Type 2 dome pyroclasts (e.g., Fig. 4e). Nanolite crystallization has been attributed to late stage crystallization in shallow regions, and cooling and oxidation as proposed by Mujin and Nakamura (2014) for Shinmoedake volcano (Japan). We note that these nanolites likely formed substrates for heterogeneous bubble nucleation, causing very high bubble number densities in some dome pyroclasts (Colombier et al. 2017a; Shea 2017; Cáceres et al. 2020).

Based on all these observations, we propose that these Type 2 dome pyroclasts originate from the exterior of the dome (carapace and talus), in which significant cooling, crystallization and hydrothermal activity took place. This interpretation is further supported by the highly similar diktytaxitic texture and presence of cristobalite in connected vesicle clusters revealed by chemical mapping in the *in situ* dome rock corresponding to the external part of the dome remnants sampled at the rim of Kilian crater (Fig. 4f, g).

Type 3 Dome pyroclasts

These pyroclasts display bands of distinct porosities enclosing variably sintered grains. These bands often consist of macro-fractures containing microphenocrysts, phenocrysts and ash particles. The size of the particles in the sintered zones differs strongly. Sintered pyroclasts are most likely relics of parts of the dome intersected by tuffisite veins, which may have acted both as fragmentation and outgassing pathways (e.g., Stasiuk 1996; Tuffen et al. 2003; Kolzenburg et al. 2012; Castro et al. 2014; Kendrick et al. 2016; Saubin et al. 2016).

Although typical of crystal-poor rhyolitic magmas, evidence of sintering in tuffisite veins has also been recently recorded in crystal-rich magmas (e.g., Kendrick et al. 2016). Sintering involves welding of ash particles in a ductile manner, but solid-state sintering has also been shown experimentally as a plausible mechanism (Ryan et al. 2018). Tuffisite veins can be generated in new fractures or use pre-existing veins (e.g., Kendrick et al. 2016). Sintering reduces both porosity and permeability with time (e.g., Wadsworth et al. 2017; Heap et al. 2019). Variable degree of sintering due to different P-T-t conditions can accordingly lead to a broad range of values of porosities and permeabilities in the tuffisite pyroclasts. Hence, tuffisite veins can initially promote outgassing during fracturing and ash-jetting stage, yet also cause dome overpressurization during the ash accumulation and sintering stages.

Fractures hosting tuffisites generally form via multiple fragmentation events and gas- and ash-explosions, as observed at Colima volcano (Kendrick et al. 2016) and during Vulcanian activity at Chaitén volcano (Saubin et al. 2016). We noted the presence of tuffisite pyroclasts in all the deposits associated with Vulcanian phases. We can therefore propose that each Vulcanian episode during the Kilian eruption was preceded by repeated fragmentation events, possibly including gas- and ash-explosions.

The variable degrees of sintering in different pyroclasts may reflect sintering at different temperature conditions in the different parts of the dome. Sintering in the colder carapace and talus regions likely occurred at lower temperature, therefore welding was less efficient and tuffisite preserved a granular, brecciated aspect (Fig. 3k, l). On the other hand, the degree of welding was higher in the interior of the dome, causing the fractures to seal almost completely, leading to the banded textures.

The glass in the non-granular groundmass of Type 3 pyroclasts is similar to that of Type 1 dome pyroclasts, but with peculiar chemical signatures (e.g., Fig. 5, 7 and 8). This may be explained by a lower crystallinity of Type 3 pyroclasts, as suggested by the XRD data (Fig. 6).

Discussion

We discuss the processes promoting outgassing versus overpressure and the implications for effusive-explosive transitions at Kilian Volcano before comparing crystallization and outgassing processes in Kilian trachyte to other silicic magmas to unravel the peculiarities of trachytic Vulcanian eruptions.

Conduit stratigraphy during the dome-forming phases of Kilian Volcano and comparison with other volcanoes

The textural and chemical transition from pumice to Type 1 to Type 2 dome pyroclasts provides insights into the stratigraphy of the conduit prior to Vulcanian episodes. As we infer the replenishment of conduit prior to a Vulcanian eruption to occur in a single batch of magma ascent (Wright et al. 2007), we propose that the differences in crystallinity between the pyroclast types reflect differences in location in the conduit rather than residence time (as proposed by Couch et al. 2003). The high crystallinity of Type 2 dome pyroclasts can be explained by (i) decompression to shallower depths, (ii) greater cooling and (iii) more extensive degassing leading to the formation of a highly viscous carapace. The parent magma of Type 1 "glassy" dome was emplaced underneath this carapace, with more limited decompression and likely absence of cooling causing less crystallization. Finally, the parental magma of the pumice pyroclasts resided deeper in the conduit at the time of Vulcanian excavation, with less decompression than in the Type 1 dome, causing lower crystallinities. The Type 3 magma was likely emplaced by granular sintering following gas and ash explosions and ensuing settling of the ash particles in the fractures. We propose a schematic representation of the dome growth at Kilian in figure 10.

We note that similar vertical pyroclast transition from pumice to glass-bearing dome and more crystal-rich dome was also observed for Soufrière Hills volcano (SHV) in Montserrat (Couch et al. 2003). Couch et al (2003) specify that the glassy dome samples have crystallinities and compositions intermediate between the pumice and crystalline dome samples at SHV. They also show that cooling only plays a role in the outermost parts of the dome (carapace). This similarity in lithology is additional evidence that the 9.4 ka Kilian Vulcanian phases were analogous to Vulcanian activity at Soufrière Hills volcano in term of conduit stratigraphy, as proposed by Colombier et al (2017a).

The model of conduit proposed here with an outermost crystal-rich carapace at Kilian Volcano contrasts with other models of plug/dome forming eruptions that commonly infer lower crystallinity in the carapace due to faster quenching (e.g., Shea et al. 2017; Zorn et al. 2018). On the other hand, similarities with previous eruptive scenarios exist. Kushnir et al (2016) and Heap et al (2018), for instance, also attribute the diktytaxitic textures observed in the Type 2 pyroclasts to a low permeability cap in the carapace and talus regions.

Outgassing vs. Pressurization in crystal-rich trachytic magmas

The products of the Kilian eruption suggest that outgassing was significant in the magma column prior to each Vulcanian phase. Outgassing was likely promoted by enhanced bubble coalescence in a crystal-rich magma (e.g., Oppenheimer et al. 2015; Lindoo et al. 2017; Colombier et al. 2020), brittle fracturing (e.g., Lamur et al. 2017) and by fracture-like and intergranular connected pore space in tuffisite veins (Type 3 dome pyroclasts; Heap et al. 2019). The dominant pathways of gas escape and fluid transport occur along interconnected vesicle clusters and tuffisite veins, and extensive precipitation of cristobalite appears to have been restricted to the exterior of the dome. We note that the usual development of shear fractures was rarely observed at the scale of the tephra, but likely had an important role on large-scale outgassing in the trachytic dome (e.g., Gaunt et al. 2014). Outgassing also occurred in the dome interior and the pumice parental magma prior to the eruption through connected vesicle networks, and occasionally led to the formation of cristobalite in the dome interior. The low magmatic water contents in the pumice pyroclasts also indicate important pre- or post-fragmentation degassing/outgassing in this population (e.g., Giachetti et al. 2015). Permeable gas escape in the pumice may occur through coalesced bubbles and bubble chains resembling fracture-like geometries described elsewhere in crystal-rich volcanic rocks and magma analogues (e.g., Heinrich et al. 2020; Oppenheimer et al. 2015; Parmigiani et al. 2016; Colombier et al. 2020).

Pressurization in the conduit prior to the Vulcanian episodes may be explained by a low magma permeability reducing gas escape and promoting the buildup of fragmentation, possibly triggering fragmentation. A low permeability may be caused by: (i) late bubble coalescence and outgassing in the hot vesicular magma underneath the lava dome, (ii) bubble collapse and isolation of the porous network in the dome, (iii) sealing of the pores by cristobalite or (iv) granular densification during sintering. Several studies suggested that occlusion of pore space by vapor-phase precipitation of cristobalite can cause a reduction in permeability, promoting gas pressurization and destabilization of the dome and explosive activity (Horwell et al. 2013; Boudon et al. 2015). The Type 2 dome pyroclasts containing cristobalite have a permeability ranging between 10^{-16} and 10^{-12} m² (Colombier et al. 2017a) implying that the presence of cristobalite is not systematically linked with complete densification in the Kilian domes. We propose that additional processes such as sintering, compaction, pore collapse and/or limited pre-fragmentation coalescence (e.g., Okumura et al. 2013; Kendrick et al. 2016; Wadsworth et

613 al. 2017; Von Aulock et al. 2017; Ryan et al. 2018) also contributed to the reduction of
614 permeability within the conduit.

615

616 **Magma ascent and rheological changes during the 9.4 ka eruption**

617 The eruption started with ascent of a low viscosity, trachytic magma with a temperature
618 T_i~775°C and an initial water content of 8 wt% from a depth corresponding to a lithosthatic
619 pressure of 300–400 MPa (Martel et al. 2013). These conditions imply to an initial melt
620 viscosity of $10^{1.71}$ Pa.s. Magma ascent from this reservoir was marked by a (i) significant
621 increase in melt viscosity up to $10^{11.07}$ Pa.s at the time of quenching of vesicular magma (that
622 is, at the glass transition temperature T_g) in the conduit at shallow levels, and (ii) a dramatic
623 loss of H_2O from 8 wt.% to 0.04 wt% inferred from the viscosity model and thermogravimetric
624 analysis. Before quenching to the glass transition, the viscosity of the trachytic melt in the
625 pumice population assuming isothermal decompression at a temperature of 775°C was $10^{9.38}$
626 Pa.s. We note that fragmentation of the vesicular magma may have occurred at or above T_g
627 giving a temperature range of 689–775°C. Decompression-induced crystallization and the
628 ensuing rise in melt SiO_2 contributed to increasing the melt viscosity significantly. Melt
629 viscosity calculated using the Giordano et al (2008) model is even higher in the dome core due
630 to more extensive crystallization and evolution towards rhyolitic composition (Fig. 5) with a
631 value of $10^{11.69}$ Pa.s at 775° C. In addition, the high crystal abundances in the magma likely
632 increased the magma bulk viscosity significantly. We suggest that these strong rheological
633 changes, coupled to efficient outgassing, were responsible for Vulcanian activity at Kilian
634 Volcano.

635 Such extensive crystallization (Fig. 6) and water loss estimates agree with previous
636 studies suggesting that both of these processes are relatively rapid in trachytic melts (e.g.,
637 Arzilli and Caroll 2013; Fanara et al. 2013; Shea et al. 2017; Arzilli et al. 2020). Effusive and
638 explosive events in andesitic and rhyolitic magmas are typically associated with ascent rates
639 lower and higher than approximately 3.6 $MPa.h^{-1}$, respectively (Cassidy et al. 2018). We
640 compiled crystallinity data as a function of depth from isothermal decompression experiments
641 of crystallization at decompression rates that are faster and slower, respectively, than the
642 explosive-effusive limit of 3.6 $MPa.h^{-1}$ (Hammer and Rutherford 2002; Szramek et al. 2006;
643 Mollard et al. 2012; Arzilli and Caroll 2013; Martel and Iacono-Marziano 2015). We find an
644 increase in the range and maximum value of crystallinity at shallow depth (< 3km) with
645 decreasing decompression rate for rhyolitic and basaltic-andesitic starting compositions (Fig.

11). We also find that the range of experimental microlite content at fast decompression rates and at shallow depth (< 3km) straddles the natural data for sub-Plinian-Plinian explosive eruptions and obsidian flows with microlite content typically lower than 50 vol% (Fig. 11; Fig. 12e). On the other hand, microlite contents for slow decompression experiments at shallow range from 5 to 100 vol% and match data for volcanic rocks from Vulcanian eruptions and crystal-rich lava domes and plugs (Fig. 11; Fig. 12e). This suggests that slow ascent rates are required for the effusive emplacement of crystal-rich lava domes/plugs, followed or not by Vulcanian activity. Interestingly, the crystallinity in rapidly decompressed trachyte is higher than in rapidly decompressed basaltic-andesites and rhyolites with high crystallinities reached at shallow depth (Fig. 11; Fig. SM1 in the supplementary material). This may imply (i) that the effusive-explosive limit may be shifted to higher decompression rates for trachytic magmas and (ii) that initially fast trachytic magmas can lead to effusive or transient Vulcanian eruptive style due to efficient microlite crystallization during magma ascent followed by stagnation of the magma column favoring outgassing, cooling and further crystallization. We note that the crystallinity profiles for experiments presented in figure 11 are also influenced by additional parameters such as variable temperatures, dwelling time at final pressure and the experimental procedure to reach this final pressure (single-step vs. continuous decompression; Gaunt et al. 2020). However, the decompression rate appears to be a major control of the near-surficial crystallinity range attained.

We compare these dynamic, disequilibrium crystallization experiments to crystallinity profiles as a function of depth calculated at equilibrium conditions (i.e., independent of kinetics) using Rhyolite-MELTS (Gualda et al. 2012). The model was run using a representative average starting bulk composition (excluding the Type 2 dome pyroclasts with cristobalite, see Table 2), and storage conditions of 350 MPa, 8 wt % H_2O and assuming isothermal decompression with a range of temperature of 755–795°C (see Martel et al. 2013). The isothermal assumption was based on the fact that cooling was limited to a maximum of 100°C before crossing the glass transition temperature and that heating related to latent heat of crystallization or friction is limited or localized to zones of high strain localization (Blundy et al. 2006; Lavallée et al. 2015). Rhyolite-MELTS runs yield crystallinities similar to the natural case for Kilian trachytes at deep (storage) and surficial (dome carapace) conditions (Fig. 11). The modelled values also compare nicely with some decompression experiments at shallow depths. However, the crystallinity profile calculated by MELTS at intermediate depth (3–8km) is significantly larger than the values obtained by decompression experiments. As a result, we interpret the crystallinity trends of the Kilian magma primarily in light of experimental data.

We infer that the Kilian magmas experienced high initial decompression rates (due to the initial low magma viscosity and high water content) which favored disequilibrium conditions. The fast crystallization of trachytic magma was nevertheless high enough for crystallization to keep pace with this rapid ascent, yielding high final crystallinities at a shallow depth in the conduit (<2 km; Fig. 11). Crystallization progressively hindered ascent and caused magma stalling at the level of the plug or dome and of the underlying vesicular magma. Assuming that the decompression rate of the volatile-rich trachytic magma was similar to the experimental rate of trachytic melt at 7–60 $MPa.h^{-1}$, we obtain a time scale of 5 to 57 hours for replenishment of the conduit and shallow emplacement of the dome and underlying vesicular magma. These ascent rates are considerably higher than those estimated for other Vulcanian eruptions at Soufrière Hills (Montserrat) and Guagua Pichincha (Ecuador) volcanoes (~0.5–2 $MPa.h^{-1}$; Druitt et al. 2002; Wright et al. 2007).

Generalization to trachytic volcanic eruptions

Small to moderate volume trachytic eruptions are often characterized by shifts in eruptive style such as dome-forming to Vulcanian styles (Kilian episodes U1, K1 and K2; Colombier et al. 2017a), Vulcanian to sub-Plinian styles (Kilian episodes U2 and U3; Colombier et al. 2017a), phreatomagmatic to Strombolian-Vulcanian (Monte Nuovo upper member, Phlegrean Fields,Italy; D'Oriano et al. 2005; Piochi et al. 2008), and obsidian dome- or plug-forming to Strombolian-Vulcanian styles (Pu'u Wa'awa'a, Hualālai volcano, Hawaii; Shea et al. 2017). On the other hand, large-volume, highly explosive eruptions of trachytic magma like the Plinian phase of the Campanian Ignimbrite eruption in the Phlegrean Fields, Italy, or the Povaçao ignimbrite in Azores, also occur (Rosi et al. 1999; Gottsmann et al. 2002; Polacci et al. 2003). This broad spectrum of eruptive style for trachytic magmas, even during a single eruption, is likely related to (i) the low viscosity of trachyte compared to rhyolite (e.g., Giordano et al. 2004; Andujar and Scaillet 2012), (ii) a slightly higher melt water diffusivity of trachytic magma compared to rhyolitic composition (Fanara et al. 2013) and (iii) the faster crystallization kinetics of trachytic magmas (e.g., D'Oriano et al. 2005; Arzilli and Caroll 2013; Shea et al. 2017; Arzilli et al. 2020). These idiosyncrasies cause first-order rheological changes in the magma and affect ascent rate, closed-system degassing, outgassing efficiency, and fragmentation behavior.

We compiled crystallinity and porosity data from the literature on intermediate to silicic volcanic rocks with a broad range of compositions and eruptive style (Fig. 12; see caption for references). We separated the crystallinity datasets in terms of crystallinity, groundmass microlite content and phenocryst content. When using the bulk and microlite contents (but not phenocryst contents), this compilation allows discrimination between pyroclasts of Plinian origin, Vulcanian origin, crystal-rich domes or plugs (and associated block-and-ash flows), and crystal-poor obsidian-bearing domes and flows. This implies that microlite content controls the crystallinity trends observed.

The tephra from Vulcanian eruptions range from relatively microlite-poor (microlite content <50 vol%) pumice pyroclasts similar to those of Plinian eruptions to microlite-rich dome and plug material, with an anticorrelation and a kink in the crystallinity–porosity trend (Fig. 12b,e). The Kilian trachytes show a similar pattern but correspond to the upper bound of microlite content of this Vulcanian trend (Fig. 12b,e). In particular, microlite-poor pyroclasts (microlite content <40 vol%) which are ubiquitous in the case of subalkaline Vulcanian eruptions are absent at Kilian Volcano. In general, we noticed that trachytic and phonolitic vesicular pyroclasts from Vulcanian to Plinian activity have a broader range of microlite content and are frequently microlite-richer than their subalkaline counterparts at a given porosity, which likely reflects the propensity of alkaline magmas to crystallize faster during ascent (Fig. 12b).

Comparing the datasets of microlite content for trachytic and phonolitic compositions offers valuable insights into potential end members of eruptive styles involving these compositions (Fig. 12d). A Vulcanian trachytic eruption involves the formation of a crystal-rich plug or dome via extensive crystallization and outgassing – a process which is possible even at ascent rates faster (i.e., higher than 3.6 MPa/h) than those inferred for dome-forming eruptions involving rhyolitic and andesitic compositions. In a scenario in which ascent is significantly faster and/or the temperature is higher, trachytic magmas may ascend without significant crystallization and erupt effusively as low viscosity obsidian plugs, domes or flows, provided that outgassing is still efficient enough (Fig. 12d; Iezzi et al. 2008; Shea et al. 2017). On the other hand, at conditions of ascent rate, outgassing, and crystallization intermediate between the Vulcanian eruptive style observed at Kilian and obsidian-forming eruptions, trachytic magmas may switch between Strombolian and Vulcanian styles, as observed at Pu‘u Wa‘awa‘a volcano (Shea et al. 2017). In such case, the tephra also display a bimodal porosity distribution (Shea et al. 2017) and an anticorrelation of crystallinity with porosity (Fig. 12d). Finally, conditions for sub-Plinian to Plinian eruptions may be met for a range of microlite content from ~0 (e.g., Campanian Ignimbrite) to up to >40 vol% (e.g., Kilian intermediate

746 phases, Vesuvius) depending on ascent rate, melt viscosity and outgassing efficiency. The key
747 observation of this compilation is that the eruptive style for a given trachytic and phonolitic
748 magmas will largely depend on the balance between the initial lower viscosity compared to
749 subalkaline magmas and the faster crystallization of microlites in the conduit during magma
750 ascent.

751

752 **Implications for the cyclicity of trachytic-phonolitic Vulcanian eruptions**

753

754 As discussed previously, trachytes are characterized by a broad spectrum of eruptive styles,
755 with frequent effusive-explosive transitions that depend mainly on ascent rate, temperature,
756 initial volatile content, crystallization kinetics, and outgassing efficiency prior to eruption. In
757 particular, high ascent rates may be compensated by rapid crystallization causing magma
758 stagnation and transient, cyclic Vulcanian eruptions. Although these eruptions bear many
759 similarities with Vulcanian eruptions involving andesitic and dacitic magmas (e.g., Soufrière
760 Hills), we suggest that the main difference may be the shorter time for conduit replenishment
761 in the case of trachytic magma. This may influence the cyclicity of these Vulcanian eruptions,
762 with likely shorter intervals between explosive pulses than observed at well-monitored andesitic
763 and dacitic volcanoes. We concur with the postulation of D'Oriano et al (2005) that the balance
764 between low viscosity and high crystal growth rates may shorten the time required for pressure
765 build up during crystallization of evolved alkaline magmas. This, coupled to the paucity of
766 observed trachytic and phonolitic eruptions, has implications for the hazard assessment of
767 future activity at alkaline volcanoes.

768

769 **Conclusion**

770 This study is an attempt to shed light on the effusive-explosive transitions during Vulcanian
771 episodes of the 9.4 ka eruption of Kilian Volcano, Chaîne des Puys, France and on trachytic
772 eruptions in general. The principal conclusions are:

773 • Initial effusive activity at Kilian Volcano was induced by rheological changes due to
774 extensive microlite crystallization causing a magma viscosity increase of up to more
775 than 10 orders of magnitude, and efficient closed- and open-system degassing.

- Outgassing occurred via bubble coalescence, brittle fracturing and through tuffisite veins sintered following gas- and ash-explosions.
- Effusive activity transitioned to explosive Vulcanian episodes due to pressurization of the dome or of the underlying vesicular magma. Processes likely to have promoted overpressure and fragmentation during the explosive phases include limited pre-fragmentation bubble coalescence and outgassing in the hot vesicular magma underneath the lava dome, bubble collapse and reduction of permeability in the dome, sealing of the pores by cristobalite, and granular densification during sintering.
- The conduit prior to each Vulcanian explosion was stratified as reflected in the pyroclasts population with a transition from crystal-rich dome pyroclasts (carapace and talus regions) to glass-bearing dome pyroclasts (dome interior) and to pumice pyroclasts (underlying vesicular magma). This lithologic sequence and conduit stratigraphy are similar to those observed at Soufrière Hills volcano, Montserrat.
- Specific properties of trachytic magmas such as high water solubility, high water diffusivity, rapid crystal growth, and low viscosity yield a wide spectrum of rheology and degassing conditions. This promotes a broad range of eruptive style and frequent effusive-explosive transitions.

Although trachytic eruptions can jeopardize highly populated areas, the eruptive processes at these volcanoes remain less constrained than their subalkaline counterparts due to the paucity of direct observations of trachytic eruptions. Future studies will be necessary to better constrain the kinetics and coupled effect of vesiculation and crystallization processes and associated textures during decompression of trachytic magmas.

Acknowledgements

MC and DBD acknowledge support from an ERC ADV 2018 Grant 834225 (EAVESDROP). This work benefited from thoughtful comments and suggestions by the two reviewers Jessica Larsen and Hugh Tuffen that helped to significantly improve our manuscript. We are thankful to the executive editor Andrew Harris and the associate editor Michael James for editorial handling and additional comments on our manuscript. This is Laboratory of Excellence ClerVolc publication number XXX.

References

Adams NK, Houghton BF, Fagents SA, Hildreth W (2006) The transition from explosive to effusive eruptive regime: The example of the 1912 Novarupta eruption, Alaska. Bull Geol Soc Am 118:620–634. https://doi.org/10.1130/B25768.1

de Andrade FRD, Polo LA, Janasi V de A, Carvalho FMS (2017) Volcanic glass in Cretaceous dacites and rhyolites of the Paraná Magmatic Province , southern Brazil : Characterization and quantification by XRD- Rietveld. J Volcanol Geotherm Res. https://doi.org/10.1016/j.jvolgeores.2017.08.008

Andújar J, Scaillet B (2012) Relationships between pre-eruptive conditions and eruptive styles of phonolite – trachyte magmas. LITHOS 152:122–131. https://doi.org/10.1016/j.lithos.2012.05.009

Arzilli F, Carroll MR (2013) Crystallization kinetics of alkali feldspars in cooling and decompression-induced crystallization experiments in trachytic melt. Contrib to Mineral Petrol 1011–1027. https://doi.org/10.1007/s00410-013-0906-1

Arzilli F, Stabile P, Fabbrizio A, et al (2020) Crystallization Kinetics of Alkali Feldspar in Peralkaline Rhyolitic Melts : Implications for Pantelleria Volcano Crystallization Kinetics of Alkali Feldspar in Peralkaline Rhyolitic Melts : Implications for Pantelleria Volcano. Front Earth Sci. https://doi.org/10.3389/feart.2020.00177

Belousov A, Behncke B, Belousova M (2011) Generation of pyroclastic flows by explosive interaction of lava flows with ice / water-saturated substrate. J Volcanol Geotherm Res 202:60–72. https://doi.org/10.1016/j.jvolgeores.2011.01.004

Blower J (2001) Factors controlling permeability-porosity relationships in magma. Bull Volcanol 63:497–504. https://doi.org/10.1007/s004450100172

Blundy J, Cashman K (2001) Ascent-driven crystallisation of dacite magmas at Mount St Helens , 1980–1986. Contrib to Mineral Petrol 2:631–650. https://doi.org/10.1007/s004100000219

Blundy J, Cashman K, Humphreys M (2006) Magma heating by decompression-driven crystallization beneath andesite volcanoes. Nature 443. https://doi.org/10.1038/nature05100

Boivin P, Thouret J (2014) The Volcanic Chaîne des Puys : A Unique Collection of Simple and Compound Monogenetic Edifices. In: Landscapes and landforms of France. pp 81–91. https://doi.org/10.1007/978-94-007-7022-5

Boivin P, Miallier D, Cluzel N, et al (2015) Building and ornamental use of trachyte in the center of France during antiquity : Sources and criteria of identification. J Archaeol Sci Reports 3:247–256. https://doi.org/10.1016/j.jasrep.2015.06.017

Boivin, P., Besson, J.-C., Briot, D., Camus, G., de Goër de Herve, A., Gourgaud, A., Labazuy, P., Langlois, E., de Larouzière, F.-D., Livet, M., Mergoil, J., Miallier, D.,

844 Morel, J.-M., Vernet, G., Vincent, P.M., Fasc., Cart., 2017. Volcanologie de la Chaîne
845 des Puys. Parc Nat. Régional la Chaîne des Puys, 5e édition (200 pp.).

846 Boudon G, Balcone-boissard H, Villemant B, Morgan DJ (2015) What factors control
847 superficial lava dome explosivity? Nat Publ Gr 1–14. https://doi.org/10.1038/srep14551

848 Cáceres F, Castruccio Á, Parada MA (2018) Morphology , effusion rates and petrology of
849 postglacial lavas of Laguna del Maule Volcanic Field , Chilean Andes , and implications
850 for their plumbing system. Geochemistry, Geophys Geosystems 19:4925–4944. doi:
851 10.1029/2018GC007817

852 Cáceres F, Wadsworth FB, Scheu B, et al (2020) Can nanolites enhance eruption explosivity ?
853 Geology 1–5. https://doi.org/10.1130/G47317.1/5074194/g47317

854 Calder ES, Kendrick JE, Bernstein M (2015) Lava Dome Eruptions. The Encyclopedia of
855 Volcanoes. https://doi.org/10.1016/B978-0-12-385938-9.00018-3

856 Cassidy M, Cole PD, Hicks KE, et al (2015) Rapid and slow : Varying magma ascent rates as
857 a mechanism for Vulcanian explosions. Earth Planet Sci Lett 420:73–84.
858 https://doi.org/10.1016/j.epsl.2015.03.025

859 Cassidy M, Manga M, Cashman K, Bachmann O (2018) Controls on explosive-effusive
860 volcanic eruption styles. Nat Commun. https://doi.org/10.1038/s41467-018-05293-3

861 Castro JM, Dingwell DB (2009) Rapid ascent of rhyolitic magma at Chaitén volcano, Chile.
862 Nature 461:780–783. https://doi.org/10.1038/nature08458

863 Castro JM, Bindeman IN, Tuffen H, Schipper CI (2014) Explosive origin of silicic lava:
864 Textural and δD-H_2O evidence for pyroclastic degassing during rhyolite effusion. Earth
865 Planet Sci Lett 405:52–61. https://doi.org/10.1016/j.epsl.2014.08.012

866 Christiansen R., Lipman PW (1966) Emplacement and Thermal History of a Rhyolite Lava
867 Flow near Fortymile Canyon , Southern Nevada. Geol Soc Am Bull 77:671–684.
868 https://doi.org/10.1130/0016-7606(1966)77

869 Clarke AB, Stephens S, Teasdale R, et al (2007) Petrologic constraints on the decompression
870 history of magma prior to Vulcanian explosions at the Soufrière Hills volcano,
871 Montserrat. J Volcanol Geotherm Res 161:261–274.
872 https://doi.org/10.1016/j.jvolgeores.2006.11.007

873 Cluzel N, Laporte D, Provost A, Kannewischer I (2008) Kinetics of heterogeneous bubble
874 nucleation in rhyolitic melts : implications for the number density of bubbles in volcanic
875 conduits and for pumice textures. Contri 156:745–763. https://doi.org/10.1007/s00410-
876 008-0313-1

Colombier M, Gurioli L, Druitt TH, et al (2017a) Textural evolution of magma during the 9.4-ka trachytic explosive eruption at Kilian Volcano, Chaîne des Puys, France. Bull Volcanol 79. https://doi.org/10.1007/s00445-017-1099-7

Colombier M, Wadsworth FB, Gurioli L, et al (2017b) The evolution of pore connectivity in volcanic rocks. Earth Planet Sci Lett 462:99–109. https://doi.org/10.1016/j.epsl.2017.01.011

Colombier M, Wadsworth FB, Scheu B, et al (2020) In situ observation of the percolation threshold in multiphase magma analogues. Bull Volcanol 1–15. https://doi.org/10.1007/s00445-020-1370-1

Couch S, Harford CL, Sparks RSJ, Carroll MR (2003) Experimental Constraints on the Conditions of Formation of Highly Calcic Plagioclase Microlites at the Soufrière Hills , Montserrat. J Petrol 44:1455–1475. https://doi.org/10.1093/petrology/44.8.1455

Damby DE, Llewellin EW, Horwell CJ, et al (2014) The α–β phase transition in volcanic cristobalite. J Appl Crystallogr 1205–1215. https://doi.org/10.1107/S160057671401070X

Delcamp A, Van Wyk De Vries B, Stéphane P, Kervyn M (2014) Endogenous and exogenous growth of the monogenetic The monogenetic Lemptégy volcano in. Geol Soc Am 998–1019. https://doi.org/10.1130/GES01007.1

De Hoog JCM, Bergen MJ Van, Jacobs MHG (2005) Vapour-phase crystallisation of silica from SiF4 -bearing volcanic gases. Ann Geophys 48:

Deniel C, Boivin P, Miallier D, Gerbe MC (2019) Multi-stage growth of the trachytic lava dome of the Puy de Dôme (Chaîne des Puys, France). Field, geomorphological and petro-geochemical evidence. J Volcanol Geotherm Res. https://doi.org/10.1016/j.jvolgeores.2019.106749

Matteo V Di, Carroll MR, Behrens H, et al (2004) Water solubility in trachytic melts. Chem Geol 213:187–196. https://doi.org/10.1016/j.chemgeo.2004.08.042

Dingwell DB, Hess KU (1998) Melt viscosities in the system Na-Fe-Si-O-F-Cl : Contrasting effects of F and Cl in alkaline melts. Am Mineral 83:1016–1021

Döbelin, N., Kleeberg, R., 2015. Profex: a graphical user interface for the Rietveld refinement program BGMN. Journal of Applied Crystallography, 48, 1573-1580. https://doi.org/10.1107/S1600576715014685

D'Oriano C, Poggianti E, Bertagnini A, et al (2005) Changes in eruptive style during the A . D . 1538 Monte Nuovo eruption (Phlegrean Fields , Italy): The role of syn-eruptive crystallization eruption (Phlegrean Fields , Italy): the role of syn-eruptive crystallization. Bull Volcanol. https://doi.org/10.1007/s00445-004-0397-z

912 Druitt TH, Young SR, Baptie B, et al (2002) Episodes of cyclic Vulcanian explosive activity
913 with fountain collapse at Soufriere Hills Volcano ,. Geol Soc London, Mem 21.
914 https://doi.org/10.1144/GSL.MEM.2002.021.01.13

915 Eichelberger, J C, Carrigan, C R, Westrich, H R, Price, R H (1986) Non-explosive silicic
916 volcanism. Nature 323:598–602. https://doi.org/10.1038/323598a0

917 Fanara S, Behrens H, Zhang Y (2013) Water diffusion in potassium-rich phonolitic and
918 trachytic melts. Chem Geol 346:149–161.
919 https://doi.org/10.1016/j.chemgeo.2012.09.030

920 Fitch EP, Fagents SA, Thordarson T, Hamilton CW (2017) Fragmentation mechanisms
921 associated with explosive lava – water interactions in a lacustrine environment. Bull
922 Volcanol. https://doi.org/10.1007/s00445-016-1087-3

923 Formenti Y, Druitt TH (2003) Vesicle connectivity in pyroclasts and implications for the
924 fluidisation of fountain-collapse pyroclastic flows, Montserrat (West Indies). Earth
925 Planet Sci Lett 214:561–574. https://doi.org/10.1016/S0012-821X(03)00386-8

926 Forte P, Castro JM (2019) H 2 O-content and temperature limit the explosive potential of
927 rhyolite magma during Plinian eruptions. Earth Planet Sci Lett 506:157–167.
928 https://doi.org/10.1016/j.epsl.2018.10.041

929 Gaunt HE, Sammonds PR, Meredith PG, et al (2014) Pathways for degassing during the lava
930 dome eruption of Mount St. Helens 2004 – 2008. Geology 947–950.
931 https://doi.org/10.1130/G35940.1

932 Gaunt HE, Burgisser A, Mothes PA, et al (2020) Triggering of the powerful 14 July 2013
933 Vulcanian explosion at Tungurahua Volcano, Ecuador. J Volcanol Geotherm Res
934 106762. https://doi.org/10.1016/j.jvolgeores.2019.106762

935 Giachetti T, Druitt TH, Burgisser A, et al (2010) Bubble nucleation, growth and coalescence
936 during the 1997 Vulcanian explosions of Soufrière Hills Volcano, Montserrat. J Volcanol
937 Geotherm Res 193:215–231. https://doi.org/10.1016/j.jvolgeores.2010.04.001

938 Giachetti T, Gonnermann HM, Gardner JE, et al (2015) Discriminating secondary from
939 magmatic water in rhyolitic matrix-glass of volcanic pyroclasts using thermogravimetric
940 analysis. Geochim Cosmochim Acta. https://doi.org/10.1016/j.gca.2014.10.017

941 Giordano D, Romano C, Papale P, Dingwell DB (2004) The viscosity of trachytes, and
942 comparison with basalts , phonolites , and rhyolites. Chem Geol 213:49–61.
943 https://doi.org/10.1016/j.chemgeo.2004.08.032

944 Giordano D, Russell JK, Dingwell DB (2008) Viscosity of magmatic liquids : A model. Earth
945 Planet Sci Lett 271:123–134. https://doi.org/10.1016/j.epsl.2008.03.038

946 Gottsmann J, Giordano D, Dingwell DB (2002) Predicting shear viscosity during volcanic
947 processes at the glass transition : a calorimetric calibration. Earth Planet Sci Lett 198:
948 417–427. https://doi.org/10.1016/S0012-821X(02)00522-8

949 Gualda GAR, Ghiorso MS, Lemons R V, Carley TL (2012) Rhyolite-MELTS : a Modified
950 Calibration of MELTS Optimized for Silica-rich , Fluid-bearing Magmatic Systems. J
951 Petrol 53:875–890. https://doi.org/10.1093/petrology/egr080

952 Hammer JE, Cashman K V., Hoblitt RP, Newman S (1999) Degassing and microlite
953 crystallization during pre-climactic events of the 1991 eruption of Mt . Pinatubo ,
954 Philippines. Bull Volcanol 60:355–380. https://doi.org/10.1007/s004450050238

955 Hammer JE, Rutherford MJ (2002) An experimental study of the kinetics of decompression-
956 induced crystallization in silicic melt. J Geophys Res 107.
957 https://doi.org/10.1029/2001JB000281

958 Harford CL, Sparks RSJ, Fallick AE (2003) Degassing at the Soufrière Hills Volcano,
959 Montserrat , Recorded in Matrix Glass Compositions. J Petrol 44.
960 https://doi.org/10.1093/petrology/44.8.1503

961 Harnett CE, Thomas ME, Purvance MD, Neuberg J (2018) Using a discrete element approach
962 to model lava dome emplacement and collapse. J Volcanol Geotherm Res 359:68–77.
963 https://doi.org/10.1016/j.jvolgeores.2018.06.017

964 Heap MJ, Coats R, Chen C, et al (2018) Thermal resilience of microcracked andesitic dome
965 rocks. J Volcanol Geotherm Res 367:20–30.
966 https://doi.org/10.1016/j.jvolgeores.2018.10.021

967 Heap MJ, Tuffen H, Wadsworth FB, et al (2019) The permeability evolution of tuffisites and
968 implications for outgassing through dense rhyolitic magma. J Geophys Res Solid Earth.
969 https://doi.org/10.1029/2018JB017035

970 Heinrich M, Cronin SJ, Torres-orozco R, et al (2020) Micro-porous pyroclasts re fl ecting
971 multi-vent basaltic-andesite Plinian eruptions at Mt. Tongariro , New Zealand. J
972 Volcanol Geotherm Res 401:106936. https://doi.org/10.1016/j.jvolgeores.2020.106936

973 Horwell CJ, Williamson BJ, Llewellin EW, et al (2013) The nature and formation of
974 cristobalite at the Soufrière Hills volcano, Montserrat : implications for the petrology and
975 stability of silicic lava domes. https://doi.org/10.1007/s00445-013-0696-3

976 Hughes EC, Neave DA, Dobson KJ, et al (2017) How to fragment peralkaline rhyolites :
977 Observations on pumice using combined multi-scale 2D and 3D imaging. J Volcanol
978 Geotherm Res 336:179–191. doi: 10.1016/j.jvolgeores.2017.02.020

Iezzi G, Mollo S, Ventura G, et al (2008) Experimental solidification of anhydrous latitic and trachytic melts at different cooling rates : The role of nucleation kinetics. Chem Geol 253:91–101. https://doi.org/10.1016/j.chemgeo.2008.04.008

Jaupart C, Allègre CJ (1991) Gas content, eruption rate and instabilities of eruption regime in silicic volcanoes. Earth Planet Sci Lett 102:413–429. https://doi.org/10.1016/0012-821X(91)90032-D

Juvigné E, Kroonenberg S, Veldkamp A, et al (1992) Widespread Alleröd and boreal trachyandesitic to trachytic tephra layers as stratigraphical markers in the Massif Central , France. Quaternaire 3:137–146.

Kendrick JE, Lavallée Y, Varley NR, et al (2016) Blowing Off Steam : Tuffisite Formation As a Regulator for Lava Dome Eruptions. Front Earth Sci 4:1–15. https://doi.org/10.3389/feart.2016.00041

Kolzenburg S, Heap MJ, Lavallée Y, et al (2012) Strength and permeability recovery of tuffisite-bearing andesite. Solid Earth 3:191–198. https://doi.org/10.5194/se-3-191-2012

Kushnir ARL, Martel C, Bourdier J, et al (2016) Probing permeability and microstructure : Unravelling the role of a low-permeability dome on the explosivity of Merapi (Indonesia). J Volcanol Geotherm Res 316:56–71. https://doi.org/10.1016/j.jvolgeores.2016.02.012

Lamur A, Kendrick JE, Eggertsson GH, et al (2017) The permeability of fractured rocks in pressurised volcanic and geothermal systems. Sci Rep 7:1–9. https://doi.org/10.1038/s41598-017-05460-4

Lane CS, Blockley SPE, Ramsey CB, Lotter AF (2011) Tephrochronology and absolute centennial scale synchronisation of European and Greenland records for the last glacial to interglacial transition : A case study of Soppensee and NGRIP. Quat Int 246:145–156. https://doi.org/10.1016/j.quaint.2010.11.028

Latutrie B, Andredakis I, Groeve TDE, et al (2016) Testing a geographical information system for damage and evacuation assessment during an effusive volcanic crisis. Geol Soc London, Spec Publ. in Harris, A. J. L., De Groeve, T., Garel,F. &Carn, S. A. (eds) Detecting, Modelling and Responding to Effusive Eruptions. https://doi.org/10.1144/SP426.19

Latutrie B, Harris A, Médard E, Gurioli L (2017) Eruption and emplacement dynamics of a thick trachytic lava flow of the Sancy volcano (France). Bull Volcanol. https://doi.org/10.1007/s00445-016-1084-6

Lavallée Y, Hess K, Cordonnier B, Dingwell DB (2007) Non-Newtonian rheological law for highly crystalline dome lavas. Geology 35:843–846. https://doi.org/10.1130/G23594A.1

Lavallée Y, Varley NR, Alatorre-Ibargüengoitia M, et al (2012) Magmatic architecture of dome-building eruptions at Volcán. Bull Volcanol 249–260. https://doi.org/10.1007/s00445-011-0518-4

Lavallée Y, Benson PM, Heap MJ, et al (2013) Reconstructing magma failure and the degassing network of dome- building eruptions. Geology 515–518. https://doi.org/10.1130/G33948.1

Lavallée Y, Dingwell DB, Johnson JB, et al (2015) Thermal vesiculation during volcanic eruptions. Nature 528:544–547. https://doi.org/10.1038/nature16153

Le Bas MJ, Le Maitre RW, Streckeisen A, Zanettin B (1986) A Chemical Classification of Volcanic Rocks Based on the Total Alkali-Silica Diagram. J Petrol 27:745–750. https://doi.org/10.1093/petrology/27.3.745

Lindoo A, Larsen JF, Cashman K V, Oppenheimer J (2017) Crystal controls on permeability development and degassing in basaltic andesite magma. Geol Soc Am 45:2–5. https://doi.org/10.1130/G39157.1

Martel C, Champallier MI, Prouteau G, et al (2013) Trachyte Phase Relations and Implication for Magma Storage Conditions in the Chaîne des Puys (French Massif Central). J Petrol 54. https://doi.org/10.1093/petrology/egt006

Martel C, Iacono-Marziano G (2015) Timescales of bubble coalescence, outgassing, and foam collapse in decompressed rhyolitic melts. Earth Planet Sci Lett 412:173–185. https://doi.org/10.1016/j.epsl.2014.12.010

Mastrolorenzo G, Pappalardo L (2006) Magma degassing and crystallization processes during eruptions of high-risk Neapolitan-volcanoes : Evidence of common equilibrium rising processes in alkaline magmas. Earth Planet Sci Lett 250:164–181. https://doi.org/10.1016/10.1016/j.epsl.2006.07.040

Miallier D, Pilleyre T, Sanzelle S, Boivin P, Lanos P (2012) Revised chronology of the youngest volcanoes of the Chaîne des Puys (French Massif Central). Quaternaire 23(4):283–290. https://doi.org/10.4000/quaternaire.6367

Miwa T, Toramaru A, Iguchi M (2009) Correlations of volcanic ash texture with explosion earthquakes from vulcanian eruptions at Sakurajima volcano, Japan. J Volcanol Geotherm Res 184:473–486. https://doi.org/10.1016/j.jvolgeores.2009.05.012

Miwa T, Geshi N, Shinohara H (2013) Temporal variation in volcanic ash texture during a vulcanian eruption at the Sakurajima volcano, Japan. J Volcanol Geotherm Res 260:80–89. https://doi.org/10.1016/j.jvolgeores.2013.05.010

Moitra P, Gonnermann HM, Houghton BF, Tiwary CS (2018) Fragmentation and Plinian eruption of crystallizing basaltic magma. Earth Planet Sci Lett 500:97–104. https://doi.org/10.1016/j.epsl.2018.08.003

1049 Mollard E, Martel C, Bourdier J (2012) Decompression-induced Crystallization in Hydrated
1050 Silica-rich Melts : Empirical Models of Experimental Plagioclase Nucleation and Growth
1051 Kinetics. J Petrol 53:1743–1766. https://doi.org/10.1093/petrology/egs031

1052 Mueller S, Melnik O, Spieler O, et al (2005) Permeability and degassing of dome lavas
1053 undergoing rapid decompression: An experimental determination. Bull Volcanol 67:526–
1054 538. https://doi.org/10.1007/s00445-004-0392-4

1055 Mujin M, Nakamura M (2014) A nanolite record of eruption style transition. Geology
1056 42:611–614. https://doi.org/10.1130/G35553.1

1057 Nakamura K (2006) Textures of plagioclase microlite and vesicles within volcanic products
1058 of the 1914-1915 eruption of Sakurajima Volcano, Kyushu, Japan. J Mineral Petrol Sci
1059 101:178–198. https://doi.org/10.2465/jmps.101.178

1060 Noguchi S, Toramaru A, Nakada S (2008) Relation between microlite textures and discharge
1061 rate during the 1991 – 1995 eruptions at Unzen , Japan. J Volcanol Geotherm Res
1062 175:141–155. https://doi.org/10.1016/j.jvolgeores.2008.03.025

1063 Okumura S, Nakamura M, Uesugi K, et al (2013) Coupled effect of magma degassing and
1064 rheology on silicic volcanism. Earth Planet Sci Lett 362:163–170.
1065 https://doi.org/10.1016/j.epsl.2012.11.056

1066 Oppenheimer J, Rust AC, Cashman K V, Sandnes B (2015) Gas migration regimes and
1067 outgassing in particle-rich suspensions. Front Phys 3:1–13.
1068 https://doi.org/10.3389/fphy.2015.00060

1069 Parmigiani A, Faroughi S, Huber C, et al (2016) Bubble accumulation and its role in the
1070 evolution of magma reservoirs in the upper crust. Nature 532:492–495.
1071 https://doi.org/10.1038/nature17401

1072 Platz T, Cronin SJ, Cashman K V., et al (2007) Transition from effusive to explosive phases
1073 in andesite eruptions - A case-study from the AD1655 eruption of Mt. Taranaki, New
1074 Zealand. J Volcanol Geotherm Res 161:15–34.
1075 https://doi.org/10.1016/j.jvolgeores.2006.11.005

1076 Plese P, Higgins MD, Mancini L, et al (2018) Dynamic observations of vesiculation reveal the
1077 role of silicate crystals in bubble nucleation and growth in andesitic magmas. Lithos
1078 299:532–546. https://doi.org/10.1016/j.lithos.2017.11.024

1079 Piochi M, Polacci M, Astis G De, et al (2008) Texture and composition of pumices and
1080 scoriae from the Campi Flegrei caldera (Italy): Implications on the dynamics of

explosive eruptions. Geochemistry, Geophys Geosystems 9. https://doi.org/10.1029/2007GC001746

Polacci M, Pioli L, Rosi M (2003) The Plinian phase of the Campanian Ignimbrite eruption (Phlegrean Fields , Italy): evidence from density measurements and textural characterization of pumice. Bull Volcanol 418–432. https://doi.org/10.1007/s00445-002-0268-4

Portal A, Gailler L, Labazuy P, Lénat J (2016) Geophysical imaging of the inner structure of a lava dome and its environment through gravimetry and magnetism. J Volcanol Geotherm Res 320:88–99. https://doi.org/10.1016/j.jvolgeores.2016.04.012

Portal A, Fargier Y, Labazuy P, et al (2019) 3D electrical imaging of the inner structure of a complex lava dome, Puy de Dôme volcano (French Massif Central , France). J Volcanol Geotherm Res 373:97–107. https://doi.org/10.1016/j.jvolgeores.2019.01.019

Preece K, Gertisser R, Barclay J, et al (2014) Pre - and syn - eruptive degassing and crystallisation processes of the 2010 and 2006 eruptions of Merapi volcano , Indonesia. Contrib to Mineral Petrol. https://doi.org/10.1007/s00410-014-1061-z

Preece K, Gertisser R, Barclay J, et al (2016) Transitions between explosive and effusive phases during the cataclysmic 2010 eruption of Merapi volcano , Java , Indonesia. Bull Volcanol. https://doi.org/10.1007/s00445-016-1046-z

Rangel E, Arce JL, Macías JL (2018) Storage conditions of the ~ 29 ka rhyolitic Guangoche White Pumice Sequence, Los Azufres Volcanic Field , Central Mexico. J Volcanol Geotherm Res 358:132–148. https://doi.org/10.1016/j.jvolgeores.2018.03.016

Rosi M, Vezzoli L, Castelmenzano A, Grieco G (1999) Plinian pumice fall deposit of the Campanian Ignimbrite eruption (Phlegraean Fields , Italy). J Volcanol Geotherm Res 91:179–198. https://doi.org/10.1016/S0377-0273(99)00035-9

Rowe M, Ellis BS, Lindeberg A (2012) Quantifying crystallization and devitrifcation of rhyolites by means of X- ray diffraction and electron microprobe analysis. Am Mineral. https://doi.org/10.2138/am.2012.4006

Ryan A, Russell JK, Heap MJ (2018) Rapid solid-state sintering in volcanic systems. Am Mineral. https://doi.org/10.2138/am-2018-6714

Saubin E, Tuffen H, Gurioli L, et al (2016) Conduit Dynamics in Transitional Rhyolitic Activity Recorded by Tuffisite Vein Textures from the 2008–2009 Chaitén Eruption. Front Earth Sci 4. https://doi.org/10.3389/feart.2016.00059

Schipper CI, Castro JM, Tuffen H, et al (2015) Cristobalite in the 2011 – 2012 Cordón Caulle eruption (Chile). Bull Volcanol. https://doi.org/10.1007/s00445-015-0925-z

Schipper CI, Mandon C, Maksimenko A, et al (2017) Vapor-phase cristobalite as a durable indicator of magmatic pore structure and halogen degassing: an example from White

1117 Island volcano (New Zealand). Bull Volcanol. https://doi.org/10.1007/s00445-017-1157-
1118 1

1119 Schipper CI, Castro JM, Kennedy BM, et al (2019) Halogen (Cl, F) and sulphur release
1120 during explosive, effusive, and intrusive phases of the 2011 rhyolitic eruption at Cordón
1121 Caulle volcano (Chile). Volcanica 2. https://doi.org/10.30909/vol.02.01.7390

1122 Scott JAJ, Mather TA, Pyle DM, et al (2012) The magmatic plumbing system beneath
1123 Santiaguito Volcano , Guatemala. J Volcanol Geotherm Res 237–238:54–68.
1124 https://doi.org/10.1016/j.jvolgeores.2012.05.014

1125 Shea T, Gurioli L, Houghton BF (2012) Transitions between fall phases and pyroclastic
1126 density currents during the AD 79 eruption at Vesuvius : building a transient conduit
1127 model from the textural and volatile record. Bull Volcanol 2363–2381.
1128 https://doi.org/10.1007/s00445-012-0668-z

1129 Shea T, Hellebrand E, Gurioli L, Tuffen H (2014) Conduit- to Localized-scale Degassing
1130 during Plinian Eruptions : Insights from Major Element and Volatile (Cl and H 2 O)
1131 Analyses within Vesuvius AD 79 Pumice. J Petrol 55.
1132 https://doi.org/10.1093/petrology/egt069

1133 Shea T (2017) Bubble nucleation in magmas : A dominantly heterogeneous process ? J
1134 Volcanol Geotherm Res 343:155–170. https://doi.org/10.1016/j.jvolgeores.2017.06.025

1135 Shea T, Leonhardi T, Giachetti T, et al (2017) Dynamics of an unusual cone-building trachyte
1136 eruption at Pu ‘ u Wa ‘ awa ‘ a , Hual ā lai volcano , Hawai ‘ i. Bull Volcanol.
1137 https://doi.org/10.1007/s00445-017-1106-z

1138 Signorelli S, Carroll MR (2002) the theoretical maximum amount of Cl in trachytic and
1139 phonolitic melts Experimental study of Cl solubility in hydrous alkaline melts :
1140 constraints on the theoretical maximum amount of Cl in trachytic and phonolitic melts.
1141 Contrib to Mineral Petrol 143:209–218. https://doi.org/10.1007/s00410-001-0320-y

1142 Stasiuk M V., Barclay J, Caroll MR, et al (1996) Degassing during magma ascent in the Mule
1143 Creek vent (USA). Bull Volcanol 117–130. https://doi.org/10.1007/s004450050130

1144 Szramek L, Gardner JE, Larsen J (2006) Degassing and microlite crystallization of basaltic
1145 andesite magma erupting at Arenal Volcano, Costa Rica. J Volcanol Geotherm Res
1146 157:182–201. https://doi.org/10.1016/j.jvolgeores.2006.03.039

1147 Tuffen H, Dingwell DB, Pinkerton H (2003) Repeated fracture and healing of silicic magma
1148 generate flow banding and earthquakes? Geol Soc Am. https://doi.org/10.1130/G19777.1

1149 van Wyk de Vries B, Márquez A, Herrera R, et al (2014) Craters of elevation revisited:
1150 Forced-folds, bulging and uplift of volcanoes. Bull Volcanol 76.
1151 https://doi.org/10.1007/s00445-014-0875-x

1152 von Aulock FW, Kennedy BM, Maksimenko A, et al (2017) Outgassing from Open and
1153 Closed Magma Foams. Front Earth Sci 5:1–7. https://doi.org/10.3389/feart.2017.00046

Wadsworth FB, Vasseur J, Llewellin EW, et al (2017) Topological inversions in coalescing granular media control fluid-flow regimes. Phys Rev E 96:0–6. https://doi.org/10.1103/PhysRevE.96.033113

Wen S, Nekvasil H (1994) SOLVCALC: An interactive graphics program package for calculating the ternary feldspar solvus and for two-feldspar geothermometry. Comput Geosci 20:1025–1040

Williamson BJ, Di Muro A, Horwell CJ, et al (2009) Magma Injection as a Trigger for Dome Collapse Eruption of the Soufriere Hills. Earth Planet Sci Lett. https://doi.org/10.1016/j.epsl.2010.03.027

Wright HMN, Cashman K V., Rosi M, Cioni R (2007) Breadcrust bombs as indicators of Vulcanian eruption dynamics at Guagua Pichincha volcano, Ecuador. Bull Volcanol 69:281–300. https://doi.org/10.1007/s00445-006-0073-6

Yoshimura S, Kuritani T, Matsumoto A, Nakagawa M (2019) Fingerprint of silicic magma degassing visualised through chlorine microscopy. Sci Rep 1–10. https://doi.org/10.1038/s41598-018-37374-0

Zorn EU, Rowe MC, Cronin SJ, et al (2018) Influence of porosity and groundmass crystallinity on dome rock strength: a case study from Mt . Taranaki , New Zealand. Bull Volcanol. doi: https://doi.org/10.1007/s00445-018-1210-8

Table and Figure captions

Table 1. Sample name, type, characteristics and methods applied for the different pyroclasts analyzed in this study. Superscript [a] refers to data taken from Colombier et al. (2017a)

Table 2. Crystallinities and glass content obtained by XRD. All other phases represent less than 2 vol % of the samples and were not considered for the analysis

Fig. 1. a) Map of the Chaîne des Puys with the trachytic domes shown in red. b) Map showing the locations of samples analyzed in this study. The blue triangles show sites of sampling of the Kilian tephra at the summit of Puy de Dôme lava dome (‘Kilian summit’) and on the southern flank of Puy de Dôme at the Coupe des Muletiers outcrop (‘Kilian Muletiers’). The white

1186 triangle in Kilian crater corresponds to an *in situ* dome rock sampled at the exterior of the dome
1187 remnants (red area) at the crater rim. The black dashed line delimits the rim Kilian crater

1188

1189 **Fig. 2.** The different types of pyroclasts erupted during Vulcanian activity at Kilian Volcano.
1190 a) Pumices in the 32–64 mm grain size fraction with beige-gray color and showing variations
1191 in density and degree of rounding. b) Dense, gray to dark-gray dome pyroclasts in the 32–64
1192 mm fraction showing a higher apparent density than pumice pyroclasts and mostly angular
1193 shapes with only a few sub-rounded pyroclasts. c) Highly vesicular, well rounded pumice
1194 pyroclast. d) Denser pumice pyroclast with less rounded shape. e) Dense dome pyroclast with
1195 breadcrusted surface. f) Type 3 dome pyroclast with banded texture

1196

1197 **Fig. 3.** Textural classification of the Kilian pyroclasts. The four main types of pyroclasts are
1198 shown: pumice pyroclasts (a-d), Type 1 (e-g), Type 2 (h-j) and Type 3 (k,l) dome pyroclasts. a,
1199 b: Highly vesicular pumice pyroclast U1-t-77 with sub-spherical vesicles. c, d: Pumice
1200 pyroclasts U1-b-63 and U1-b-71 with lower porosity, higher crystallinity and degree of vesicle
1201 deformation. e-g: Type 1 dome pyroclasts U1-b-97 and K1-s-2 with low porosity, high
1202 crystallinity and interstitial glass between feldspar microlites. h-j: Type 2 dome pyroclasts U1-
1203 b-96, K1-s-3 and U1-t-6 with diktytaxitic texture and presence of cristobalite in the
1204 interconnected vesicle clusters. Ellipsoids mark areas where cristobalite is observed. k, l: Type
1205 3 dome pyroclast PB11-1803-2c with granular material in between bands of variable porosity

1206

1207 **Fig. 4.** Specific textural features observed in the trachytes. Images a to f are back-scattered
1208 electron images, and images g to i are compositional maps. a: Pumice pyroclast K1_t_1 with a
1209 zoom on a fracture-like chain of coalesced vesicles in the right panel. b: Fracture-like chain of
1210 coalesced vesicles in the Type 1 dome pyroclast K2Mul3. c: Type 1 dome pyroclast
1211 PB11_1803_2b1 showing trachytic texture with aligned microlites. d: Oxide nanolites in the
1212 interstitial glass between feldspar microlites in Type 1 dome pyroclast U1-b-97. Due to
1213 limitations in image magnification, nanolites appear as bright dots only 1 or 2 pixels in width
1214 in this pyroclast and arrows are to guide the eye towards regions with high nanolite
1215 concentration. Note that the nanolites should not be confused with microlites (larger than 1
1216 µm). e: Oxide nanolites in the interstitial glass between feldspar microlites in the Type 2 dome
1217 pyroclast U1-b-96. Nanolites are commonly arranged as rims around the feldspar microlites in

this sample. f-i: scanning electron microscope images and chemical map for Si, K and Ca in the *in situ* dome rock BPK-1 sampled at the exterior of the dome remnants of Kilian crater. This dome rock has a Type 2 characteristic diktytaxitic texture with presence of cristobalite evidenced in the chemical map of Si (g)

Fig. 5. Total alkali versus SiO2 diagram showing whole rock compositions of the pyroclasts (red squares) and glass compositions of pumice pyroclasts and Type 1 and 3 dome pyroclasts. This diagram was modified after Le Bas et al. 1986. Glass is absent or rare in the Type 2 dome pyroclasts explaining the lack of data for this pyroclast population. The solid and dashed curves correspond to the evolution of melt composition during crystallization modelled using Rhyolite-MELTS at 755 and 795°C, respectively. The modelled trend was separated according to magma crystallinity (Φ_x): 0–40 vol% (red shaded area); 40–70 vol% (typical of pumice population; orange shaded area) and 70–85 vol% (typical of dome pyroclasts; blue shaded area). The inset on the right represents a feldspar ternary made using the data along with isotherms calculated using SOLVCALC (Wen and Nekvasil 1994). Ab: Albite; Olig: oligoclase; And: Andesine; Lab: Labradorite; Byt: Bytownite; An: Anorthite; San: Sanidine. Error bars are smaller than symbols

Fig. 6. a) Crystallinity (vesicle-free) vs. porosity in the pyroclasts. Orange stars, blue crosses and blue open squares represent data obtained by 2D image analysis for pumice pyroclasts, Type 1 and Type 2 dome pyroclasts, respectively (Colombier et al. 2017a). Orange circles, blue triangles, dark blue diamonds and open diamonds represent XRD data from this study for pumice pyroclasts, Type 1, Type 2 and Type 3 dome pyroclasts, respectively. The porosity data were obtained using an immersion technique based on Archimedes principle with negative error bars of 7 vol% corresponding to the maximum difference observed with the glass beads method (showing systematically lower values) for most pyroclasts (Colombier et al. 2017a). b) Porosity histogram showing the dome and pumice populations overlapping

Fig. 7. Compositions of whole rocks, interstitial glasses, melt inclusions and crystals. The interstitial glass compositions are for pumices, Type 1 and Type 3 dome pyroclasts. Glass is absent or rare in the Type 2 dome pyroclasts. Error bars are smaller than symbols

Fig. 8. Evolution of interstitial glass composition with whole pyroclast porosity. Orange circles: pumice glass. The dashed boxes show the range of porosities observed in the heterogenous Type 3 dome pyroclasts

Fig. 9. Results from the simultaneous thermal analysis showing the quantification of the glass transition temperature using differential scanning calorimetry (a) and the mass loss related to meteoritic water content using thermogravimetric analysis (b). No significant water loss is observed after T_g is crossed, consistent with the results of the viscosity model indicating low magmatic water content. The raw data are presented without baseline correction due to the weak signal during analysis

Fig. 10. Conceptual model showing the textural and chemical evolution as a function of conduit stratigraphy during effusive-explosive transitions at Kilian Volcano. The sketch illustrating dome emplacement is not to scale although the contours of the dome and pre-existing topography were inspired from geophysical studies in the area (Portal et al. 2016) and numerical models of endogenous dome growth (Harnett et al. 2018). The possible evolution of magma crystallinity and melt SiO_2 content based on the XRD and microprobe data are illustrated as a function of vertical position above the conduit. The color code was chosen to illustrate the relative temperature variations (grey: colder; orange: intermediate; red: hotter). Tuffisite veins are unrealistically wide for illustration. A cryptodome intrusion causing an uplift of the Puy Grosmanaux scoria cone and possibly associated to Kilian eruption (Van Wyk de Vries et al. 2014) is here omitted for simplicity

Fig. 11. Evolution of crystallinity with depth from storage region to atmospheric pressure during the Kilian dome-forming, Vulcanian phases. The experimental data correspond to isothermal decompression-induced crystallization experiments on basaltic-andesitic and rhyolitic melts with fast (>3.6 $MPa.h^{-1}$) and slow (<3.6 $MPa.h^{-1}$) decompression rates, respectively (Hammer and Rutherford, 2002; Szramek et al. 2006; Mollard et al. 2012; Iacono Marziano and Martel, 2015) and on trachytes at fast decompression rate (>3.6 $MPa.h^{-1}$; Arzilli and Caroll, 2013). Equilibrium crystallization conditions are shown with a modelled crystallinity profile using Rhyolite-MELTS at 755°C and 795°C and by crystallization experiments at storage conditions of Martel et al (2013). The shaded areas correspond to the

depth-crystallinity conditions for the storage region (Martel et al. 2013; Colombier et al. 2017a), the pumice population and lava dome (few hundred meters thick and with its surface at atmospheric pressure). A hypothetical range of depth is illustrated for the magma underlying the lava dome (pumice population) by matching the minimum and maximum crystallinity observed in the pumice pyroclasts with similar experimental values obtained for trachytes by Arzilli and Caroll (2013). Error bars for crystallinity are given in figure SM1 in the supplementary material

Fig. 12. Compilation of porosity and bulk, microlite and phenocryst contents for silicic volcanic rocks of different eruptive styles (Christiansen and Lipman 1966; Hammer et al. 1999; Nakamura 2006; Adams et al. 2006; Mastrolorenzo and Pappalardo 2006; Clarke et al. 2007; Lavallée et al. 2007; Noguchi et al. 2008; Piochi et al. 2008; Castro and Dingwell 2009; Miwa et al. 2009; Castro and Dingwell, 2009; Neil et al. 2010; Giachetti et al. 2010; Burgisser et al. 2010; Shea et al. 2012; Scott et al. 2012; Castro et al. 2013; Miwa et al. 2013; Innocenti et al. 2013; Nguyen et al. 2014; Rotella et al. 2014; Cassidy et al. 2015; Preece et al. 2016; Hughes et al. 2017; Latutrie et al. 2017; Colombier et al. 2017a; Shea et al. 2017; Rangel et al. 2018; Zorn et al. 2018; Cáceres et al. 2018; this study). a to c: All compositions are included. d: Only microlite data for trachytes and phonolites are shown. e: Frequency histogram showing the distribution of microlite content for the different eruptive styles and highlighting the absence of low microlite content at Kilian compared to sub alkaline Vulcanian eruptions. N is the total number of pyroclasts analyzed from the different studies included in the frequency histogram. To allow comparison between all the different studies, microlite content were corrected from phenocryst content and porosity when needed and therefore correspond to groundmass microlite contents

R: We are grateful to the Editor and the Reviewers for their very interesting comments on our work. It is rare to have such a thorough review with so many relevant comments from the reviewers so we dedicated much time to treat each comment in detail and to rebuild our manuscript around these. We believe that this review allowed us to strengthen significantly our manuscript. We here provide a response, point by point, to editor and reviewers comments where our replies appear in red.

We also provide a modified version of the manuscript with changes made after these comments appearing in yellow. In addition, we also made a number of additional changes which, we believe, improved the quality of the manuscript.

Editor's and reviewers' comments:

Editor:

The reviewers have provided two thorough and positive reviews of your paper, and clearly value its contribution. My reading of the work is in agreement, and I have appreciated the quality of the writing.
Nevertheless, the reviewers have a good number of important points to address that will greatly improve the paper in terms of rigour and clarity. Some of the comments require additional work and I encourage the authors to consider them all in detail.

R: We agree with the Editor and considered all comments of this review in detail.

The current article is >12,000 words, which exceeds the BV limit (7000) by some margin. We have flexibility, and I am not asking for a trim to 7000, but when revising, I request that everything is done to make the paper as concise as possible. Please consider this for all elements, e.g. review whether all your tables are critical to have in the main text, or whether some aspects could be moved to supplemental material.

R: We agree with the Editor and tried to simplify/clarify as much as possible. However, the comments from reviewers implied significant modifications and additions and did not allow us to shorten the manuscript. We also had to add new figures as requested by reviewer 2. We also made some important additions to the manuscript and dataset that better support our interpretations of textures (for example, the addition of in situ, carapace-type dome sample with some chemical mapping information).

We tried to shorten the irrelevant parts of the text where possible and moved several parts and the two tables in the supplementary material to shorten the main text. Unfortunately, despite these efforts the new manuscript is now longer than the previous version. We are sorry about this and hope that this is still in the range of BV flexibility.

I have only editorial/formatting comments to add to the reviewer comments, and they reflect the BV style as given in the Instructions for Authors. For a revised manuscript, please follow the detailed instructions
here: https://www.springer.com/journal/445/submission-guidelines
Example (not exhaustive) points to consider specifically are -

Level 2 heading is normal font (not italic).

R: Corrected

Numerical ranges should be separated with an en-dash, not a hyphen.

R: Corrected

References must be accepted to be included in the reference list.

R: All are now accepted

Although most references in the reference list are formatted correctly there are a number of deviations and incomplete references. Please check through for consistency and completeness.

R: We checked the references

Figures:
Please start figure captions with Fig. not ‘Figure’. Note that captions end without punctuation.

R: Corrected

Provide tables as editable tables in your word processor rather than images; don’t use commas as decimal separators or Excel-style ‘E’ notation.

R: Done. We note that two tables related to chemical analysis are now in the supplementary Table

Check all figures to ensure that, when reproduced at final size, all text is a minimum of 8 point. You can de-clutter multi-panel graph figures by not repeating labels etc. unless needed.

R: Checked

Reviewer #1 (Jessica Larsen):
General comments: Overall, I really enjoyed reading this manuscript. I find it to be very well-written, clear, and straightforward. The data in most cases support the discussion and conclusions. The data used make sense, and seem to fit in well with the aims of the study.

R: We thank the reviewer for this positive summary of our work and for all the critical points raised in the review.

I do have a few concerns about how errors are handled (see below), which need to be addressed to improve the rigorousness of the data presentation.

R: See our reply to this specific point below.

Also, the final sections of the discussion section are confusing and not well connected to the figures. I found it difficult to fit the broad discussions of eruption style together with the figures, to see a clear picture of how the particular eruption they studied could be quantitatively compared with other work. I suggest that the authors consider re-focusing this part (from Line 609 to the Conclusions section) and to tighten up and better quantify the comparison with the other studies representing a range of eruption styles. Or, the authors could just keep the discussion and conclusions focused on the more novel aspects of trachyte viscosity, crystallization, ascent rate and the Vulcanian eruption style - as observed at Kilian volcano specifically - and omit the broader comparison with Plinian, Strombolian, etc eruptions in general. It is a nice story on it's own, and can be broadened out to compare just with other Vulcanian systems without making the stretch to all the other eruption styles too.

R: We agree with the reviewer that this part was a bit confusing. We modified it and decided to keep this broad comparison of eruptive style as the other reviewer thought it was an interesting part.

To address this comment, we completed our compilation with additional data and organised the main observations in a more structured way. The key information of this compilation is that trachytes and phonolites have in general a higher microlite content for a given eruptive style (now nicely shown in figure 12 b and e). This is observed for Vulcanian and Sub-Plinian to Plinian datasets. That mirrors nicely a similar observation for the compilation of experimental data, where we observe that for a similar decompression rate trachytic melts grow much more microlites as their subalkaline counterparts (see figure 11 in the manuscript and figure SM1 in the supplementary material).

New panel d of figure 12 shows a conceptual way to discriminate between eruptive style for a given magma composition (here trachytes and phonolites) using porosity and microlite content.

We also modified the text in lines 724-729, 744-750 and additional places in order to better reflect the key observations, which are (i) the propensity of trachytic-phonolitic magmas to grow microlite faster during ascent and (ii) the subsequent ascent rate-degassing-crystallization conditions required to explain the variety of eruptive styles during trachytic eruptions.

The writing quality is excellent and I don't have any editorial comments to make. I did not find any typos or grammar issues. I did not check all of the references so the

authors should be sure that they are all included in both the text and references section consistently.

R: We checked the references

Lines 244-252: XRD results on the samples are described, with relative phase proportions for each mineral indentified. While XRD is really good at determining the types and proportions of phases present in a sample, it can be a little tricky if the strongest diffraction lines from two different minerals are close to each other in D-spacing. In that situation, it might look like a phase is missing or is even in a lower proportion relative to the more strongly scattered diffraction line. I think that the authors should include a summary of the diffraction lines and relative intensities from each phase that they used to determine phase proportions, either in Table 4 if there is room or as an electronic supplement if not. This can show how robust the phase proportions are as determined from the raw diffraction data. An example of one of the diffraction patterns could also be shown in the supplement.

R: We guess that the reviewer has the RIR method in mind, which is based on the relative CRD peak intensities. However, we used the Rietveld method, which is based on a whole pattern evaluation. In order to indicate the reliability of the Rietveld refinement we added the chi^2 values in Tab. 2 (previous table 4).

Lines 300-305 and Figure 6, Figure 6 caption - The glass transition constraints are described as an approximation (using the ~ symbol). In the figure, the scans are presented, and described in the caption as showing a "weak" signal. What are the errors associated with this data? I am admittedly not experienced with this method. However, I think an estimation of error on the cited glass transition temperatures described is needed. Otherwise, it is difficult to determine whether 692 C is significantly different than 707 C, or whether they are essentially the same, within error. This may seem like a small detail, but I think that error estimation is needed in any rigorous scientific study.

R: The error on the glass transition peak is +/- 3°C (Kai Hess personal communication). We only kept the signal corresponding to the pumice clast U1-t-77 as it was the one with best signal during thermal analysis. For the other pumice clast, the Tg region is clearly observable (from ~500 to 750°C) but we see no obvious Tg peak. Therefore, we now only discuss a value of 689°C for Tg. 707°C is outside of the experimental error but is still close enough.

Lines 300-305 - an additional comment - the numbers cited in the text and referred to Figure 6 for Tg do not match. In Figure 6, the two temperatures shown for two pumice samples are 678.8 and 689.2 C - where do the ~690 and 707 C cited in the text come from? The precision and significant figures cited in the text should match what is shown in the figure.

R: This is now figure 9. We took the value of 689 as more realistic because this curve is the one with the best signal. We now mention this in the caption. For the model, we used the data of PVC which has a similar composition to our trachytes, and a similar Tg (707°C is for this study, and is not significantly different to 690°C).

Line 454 - I am not sure what is meant by "ash-flow" explosion. Please explain?

R: This is not correct indeed. We meant gas- and ash-explosions. We removed flow

Lines 609-622 - I see the desire to enfold the results from the study into a larger scale examination of variations in eruption style in trachyte magmas versus all other magma compositions. However, I feel like this paragraph needs to be reconsidered. It does not really tie the study results specifically into other studies. It is very broad, and not well focused. Also, there are some statements that don't really hold up well. For instance, Lines 615-617 talk about how the diversity in eruption styles relative to rhyolites is explained by its lower viscosity. Yes, that may be true in some regards. However, rhyolites also can show a big range of diversity in eruption styles even within a single eruption, and time period with an eruption. A great example is Chaiten (simultaneous effusive and explosive activity), as reported by Castro et al., 2012 and Saubin et al., 2016.

R: We agree that rhyolites also show a range of eruptive style, however it is to our opinion less broad as for trachytes. Here we discuss eruptive styles including Strombolian (not discussed for rhyolites or maybe some peralkaline rhyolites), Vulcanian (here more similar to SHV with a crystal-rich plug/dome than to Chaiten where obsidian domes/flows were involved), Plinian and caldera-forming and obsidian flows (these last 3 cases also happen in rhyolitic eruptions). It seems that trachytes are more prone to large variations in eruptive style compared to rhyolites. Furthermore, the reasons for broad variations in eruptive style seem different in each compositional case. We now clearly show that the balance between lower viscosity and the propensity to grow microlite faster is the key for the eruptive style of trachytic magmas. This is now evident in figure 12, which shows the range of microlite content plots at higher values for trachytes and phonolites for a given eruptive style.

Basalts, more rarely, can also show broad variations even in a single eruption episode.

R: We agree, but basalts should be treated separately because of their much faster crystallization kinetics. We here focus on the comparison alkaline-subalkaline for intermediate to silicic compositions. Heinrich et al (2020) showed a similar compilation for basaltic to basaltic andesitic magmas and also found that microlite growth is crucial to explain Sub-plinian to Plinian eruptive style for mafic magmas. On the other hand, we are not aware of basaltic Vulcanian activity.

Maybe I am not seeing the point being made, but I suggest either deleting this paragraph, or refocusing it to be pretty specific about how their results tie into the

grander discussion of variations in eruption style across a broad range of magma compositions, as a function of viscosity primarily.

R: We hope our changes helped to clarify this part. See our previous reply on how we modified this whole section.

Lines 623-647 - These two paragraphs are a little hard to follow also. They link with Figure 9 to discuss dominant crystal content (microlites are predominant), and variations in eruption style, primarily comparing trachytes and phonolites. I had a difficult time piecing apart the descriptions of varying ascent rate with the data shown (crystallinity versus porosity). My guess is that crystallinity is used as a proxy for ascent rate? In the legend, they link the different symbols to different named eruption styles instead. I just found this to be confusing. Figure 9 needs a legend for sure, and that might help a little. I also think that a more clear link between the crystallinity and porosity data shown with ascent rate and/or stalling of magma at shallow depths might help connect back to the prior discussion about the 3.6 MPa/hour threshold? Anyway, it just is confusing to me as presented and I am not really sure about the aim of Figure 9 or the text that goes along with
it in terms of the outcomes of this study.

R: We modified this section. See our previous reply. We added a legend to figure 9.

Conclusions section - Consider taking this out of bullet format and using standard paragraph structure. It's probably just my own preference, but I think conclusions sections work better when they are written in paragraph format. If the discussion is shortened as above, the conclusions could even be expanded a bit to be more specific and quantitative.

R: We preferred to keep it as bullet points as the points discussed are rather specific and not always linked together.

Figures and data in general - I not that error bars are not included in any of the figures. Even if the data shown are single points, there should be some indication of analytical precision shown - even as a representative error bar. It is necessary to include error information so that the trends discussed in the data can be evaluated as significant or not.

R: Errors for EPMA are smaller than 1 %. We say in the relevant captions that the symbols are larger than error bars (Fig 5, 7 and 8). We added errors for porosity (Fig 6 and 8) and crystallinity (Fig 6) measured by XRD (based on a calibration now shown in the supplementary material).

Figure 1 - the text refers to lettering in the photomicrographs presented in Figure 1, but the figure does not appear to be labeled as such. Also, the scale bars in Figure 1 show different font types - those should be made all the same font for a uniform appearance.

R: We modified this figure (now figure 2).

Figure 8 - I suggest labeling the boxes that indicate the storage conditions and the dome carapace crystallinity range. Make the shading different and/or label the boxes so that they are distinguishable just by looking at the figure.

R: Agreed (now figure 11). We added a legend to the figure and use different shading for storage, pumice and dome.

Figure 9 - needs a legend so that the symbols can be more easily examined in the context of the data ranges shown.

R: We modified this figure that now includes a legend (now figure 12)

Reviewer #2 (Hugh Tuffen) :

Review of Rheological change and degassing during a trachytic Vulcanian eruption at Kilian volcano, Chaîne des Puys, France by Colombier et al

General comments

This is a strong paper, is novel, and of significant interest. I recommend for publication in BV. The dynamics of trachytic eruptions remain poorly understood and the data presented here gives useful new insights into magma ascent and evolution in trachytic eruptions. The compilation of data from experiments and other silicic eruptions is interesting, and is well integrated with the new data presented here for Kilian volcano.

R: We thank the reviewer for this positive introduction and all the constructive comments on our work. That helped us a lot.

I have made quite a large number of comments in the detailed list below. The most important, which I would like to see thoroughly addressed in your revision, are the following:

1. Please provide much more information on the eruption itself. A map showing the broader setting of the Chaine des Puys, and a detailed look at Kilian crater. Please also provide a figure showing the stratigraphy of the Vulcanian deposits, and typical clasts so we can get an impression of their size.

R: We initially did not include so much information to avoid repeating what is said in Colombier et al (2017a) but we now agree with the reviewer that an additional figure will help the reader. We provide additional information on the eruption, sample location (we also note that we added a new sample coming from the *in situ* dome located in the Kilian crater). We also discuss more in detail the possible distal deposition of Kilian tephra in central Europe. We provide a new figure 1 showing the CdP, Kilian crater and deposits on the Puy de Dôme and sample location. For the stratigraphy, however, we

refer to Colombier et al., 2017 in line 138 for a detailed description of the deposits and associated eruptive sequence, because we already have 12 figures and the Editor requested that we try to shorten the manuscript as much as possible. Regarding the clasts, we provide an additional figure with main macroscopic information (figure 2).

2. Please take a more careful look at the inferred water concentration on fragmentation (or at Tg – not necessarily the same temperature). The TGA data could give useful insights if split into sub- and supra-Tg bins. The current method of estimation based on calculations of another composition is circuitous at best.

R: The supra-Tg bins show that there is no water loss above Tg. There seems to be a slight decrease but the values are within the instrument resolution so this is negligible (error range of measurements of approximately +-100 ppm). This is consistent with the value of 0.04 wt % obtained using the viscosity models.

3. We need more constraints on vesicle deformation if this is going to stay in the paper. There are only a couple of SEM images provided, and nothing quantitative, to support the assertion that there are variable degrees of vesicle deformation in different clast types. Ideally we'd see a brief analysis of bubble aspect ratios in representative samples, to prove that there are systematic differences.

R: We did not add quantification of vesicle shape, but add a figure showing this statement qualitatively. We removed the discussion part related to this topic.

4. Could you also plot, for the experimental compilation in Fig. 8, the crystallinity as a function of decompression rate? Simply faster/slower than 3.6 MPa/h-1 is a very crude separation.

R: We thank the reviewer for this piece of advice. We now add such a figure in the supplementary material. It nicely shows that trachytes produce more crystals for a given decompression rate. And the 3.6 MPa.h-1 is a useful separation based on Cassidy et al that match the compilation data.

What happens if you plot crystallinity vs decompression rate over a small number of binned depths (e.g. 0-2 km, 2-4, 4-6, 6-8)? This would reveal a lot more about links between attained crystallinity and decompression rate, and probably support your assertions.

R: The figure becomes too messy, so this option was not taken.

5. Please separate andesite from rhyolite in your compilation of experimental crystallinities. These magma types have significantly different diffusivities, water solubilities and viscosities –andesite could be intermediate between rhyolite and

trachyte. Exploring this compositional dependence in more detail will help you make your model more generally applicable across silicic magmas.

R: We do this in the figure in supplementary material. By the way, it is in fact a basaltic andesite + different rhyolites. We corrected this. In the supplementary figure, we see that trachyte crystallizes faster than both rhyolite and basaltic andesite. We did not separate andesite from rhyolite in figure 11 to avoid confusion (anyway the trend for rhyolite and basaltic andesite as a function of decompression rate follows a similar pattern).

6. There is a mismatch between estimates of crystallinity from simple MELTS models and those in your samples. Please explore and discuss the scope for Stokes settling of crystal phases during magma ascent, and relate this to the compositional trends presented in Fig. 4. The initial melt viscosity is exceptionally low for a silicic magma, and would permit rapid settling, and thus provide scope for separation of phenocryst phases. However the viscosity drastically increases on degassing. Is there a “sweet spot” where significantly large phenocrysts have grown, and the melt viscosity is still relatively low, in which settling can occur? This should be possible at the lower end of the spectrum of ascent rates.

R: This is an interesting suggestion. The Stokes law is based on density difference. The density of the Feldspar phenocrysts (mostly oligoclase composition) is around 2650 kg/m³ which is very similar to that of the melt (2630 kg/m³). Using the initial viscosity of 10^1.71 Pa.s given in the text, this would give a displacement of 2cm/hour for a crystal of 5mm diameter. This is a maximum value assuming there is no increase of viscosity due to degassing and crystallization during this time. Considering that the replenishment of the conduit and shallow emplacement of the dome took 5 to 57 hours, crystals could not settle more than 0.1 – 1 m. A more detailed assessment is however precluded by the fact that the crystal densities modelled by MELTS are systematically lower than 2600 kg/m³, which would cause the crystals to rise buoyantly instead of settling. We are thus in a gray zone close to neutral buoyancy in the reservoir region and any settling or rising tendency would be neutralized by the increase in melt viscosity during ascent. So although we agree with the reviewer that there is a compositional trend in the whole rock data that seems related to the Feldspar population, there is sadly no easy way to prove whether it is due to differences in feldspar abundances caused by settling or floatation or to natural variability in Feldspar compositions between clasts.

Finally, we expect to have a mismatch of crystallinity at the intermediate depths where magma is rising rapidly and not stalling because of the ensuing disequilibrium conditions. The only conditions at which we expect the crystallinity to match the modelled ones is when there is enough time for crystallization (that is at the storage level and in the dome where the magma is not rising rapidly and therefore in equilibrium). We note that the MELTS output at 795°C at the storage conditions overlaps with the phenocryst content measured by Colombier et al 2017 and Martel et al. 2013 (3-20 vol%). Therefore, we propose that the difference between MELTS and

natural textures is not an issue at the storage conditions. The same is observed close to atmospheric pressure where the dome crystallinity range straddles the modelled crystallinities.

7. Figure 1 needs attention – there are far too many panels, it needs properly labelling (a, b, c, d etc.), and features of interest need to be indicated, e.g. cristobalite.

R: We now split this figure in two new figures allowing to better illustrate all the textural features (figure 2 and 3).

Specific detailed comments (relate to comments and edits to the annotated .pdf)

L19 is there truly an explosive-effusive transition during a Vulcanian phase, or simply effusion punctuated by discrete explosive events?

R: This is an interesting comment and I guess we have all different opinions on this. Some people consider the events as being mostly explosive, some as rather effusive, and other as transitional. The fact that we often find two clast populations during Vulcanian eruptions (dome + pumice) implies that we have an initial effusive activity and that this effusive material is then ejected with the underlying magma during an explosive phase. I would say the same for Strombolian eruptive style, where a degassed plug stalls close to the surface and is then erupted with the magma underneath during small explosions.

I think effusive-explosive transitions can be seen at different timescales from hours to weeks for Vulcanian eruptions to cycles lasting hundreds of years at other volcanoes.

On the other hand, we agree that discrete gas- and ash-explosions should not be considered as a transition but more a pulsatory regime as proposed by the reviewer. But here we discuss the evacuation of the conduit including both (a big part of) the effusive dome and the underlying magma so this is not a discrete event.

L23 rapid ascent and high viscosity both hinder efficient gas escape, so "subsequently" is not appropriate. an explanation needs to be sought for the ability of the gas to escape such viscous magma.

R: We removed “subsequently”. We note that bubble coalescence occurs earlier and the percolation threshold is reached at lower porosity in highly viscous magma than for

a less viscous magmas of the same crystal content, because of different regimes of bubble growth and coalescence (see Colombier et al. 2020). Therefore, gas escape can be indeed promoted in a highly viscous magma.

L25 between Vulcanian explosions?

R: We modified to “effusive activity at the onset of Vulcanian episodes”. We cannot say between Vulcanian explosions because there was some Subplinian phases recognized in the intermediate layers of the stratigraphy, between Vulcanian deposits (Colombier et al., 2017).

L29 rewrite - remove "on the other hand".

R: Done

L32 need to explain why delayed coalescence drives overpressure.

R: We replaced delayed by limited pre-fragmentation coalescence. A large part of the coalescence could be syn- or post-fragmentation based on observed textures. If there is no efficient pre-eruptive coalescence in the pumice population then that impedes gas escape and promotes overpressure.

L35 from a combination of characteristics of trachytic magma, that include...

R: Done

L37-40 some more connections are needed to bring this together. firstly, is an "effusive-explosive transition" actually simply dome growth with superimposed Vulcanian events? for me the transition is the overall change in style, e.g. subplinian-Vulcanian-lava dome growth with/without ash venting. Pulsatory activity is not a transition.

R: See my previous reply on this point above. The first arrival of magma at the surface is not explosive and consists of effusive dome formation. Furthermore, several studies speak about effusive-explosive transitions for this eruptive style (e.g., Druitt et al., 2002).

secondly, it is implied here that there is a relationship between the inter-event rate of Vulcanian explosions and the effusion rate. This needs to be clearly spelt out, justified, and supporting citations given.

R: This is simply based on the results of the compilation and our discussion.

L54 these are not explosive-effusive transitions, they are pulses of pressurisation of the upper conduit and dome.

R: See our previous reply to this comment. We rephrased to show that we do not mean only discrete explosion of the lava dome but rather explosive activity and evacuation of the whole conduit.

L64 2019

R: Corrected

L84 change to "than"

R: Corrected

L117-118 change to “identify their eruptive style controls”

R: Done

L119-121 do you mean to say that this eruptive style was only possible because it was a trachytic composition - so, for example, an andesite or phonolite would not exhibit such behaviour? the way it is written suggests that there were only rheological changes because it is trachyte, but we know that the rheology of other magma compositions also changes during ascent!

R: We agree with the reviewer that similar changes may occur but at different timescale for other compositions. Therefore we now specify “rapid rheological change” and “the kinetics of effusive-explosive transitions”.

L132 for me the explosive-effusive transition would relate to this big picture, e.g. from subplinian via Vulcanian towards more purely effusive activity - as conceptualised in Castro et al 2014 EPSL when writing about Chaitén 2008-09

R: See my previous replies on this comment.

L130-133 refer to a map figure of the C de P

R: We now add a new figure.

L169 check capitalisation in this sentence

R: Done

L176 comment on likelihood of hydration changing major element composition when corrected to 100 %?

R: We showed by calorimetry that we had rehydration of the samples analysed by EMPA. This may be the cause that the totals are below 100, as explained in lines 192.

L182 not sure what a negative mesh and 99.5 % mean!

R: The mesh value is related to grain size, we removed this information as it was not relevant. 99.5% represents the chemical purity of Silicon. We specify it in line 202.

L191 lower case numbers

R: Done

L206-207 need to refer to a new figure - show where the samples were collected from, and ideally a stratigraphic log showing the progression of the eruptive episodes, and where these analysed samples fit in.

R: We added two sentences on the sample location in line 156. For the log we refer to the figure 3 of Colombier et al., 2017 and add a sentence in lines 138 to tell the reader that there is more information there. We already have 12 figures and we do not want to repeat too much the previous study.

L206-207 also, can we please hear more about the pyroclastic deposits - thickness, volume, areal extent, componentry, distance from vent, clast sizes and nature?

R: Again this is all discussed in Colombier et al., 2017. We add a sentence on dispersal in line 149 and some macroscopic description of the clasts in line 234.

L211 please also tell us the sizes of the pumice clasts - there is nowhere near enough context for these detailed textures. Also need to label Fig. 1a, e, m, etc..

R: Most of the clasts are lapilli in the 16-32 mm fraction with a few samples in the fraction 32-64mm. This is now specified in line 231 and shown in Table 1.

L213 needs better labelling and explaining. can we be talked through Fig. 1 better, and have it explained what we are looking at?

R: We now separate this figure in two figures (3 and 4). We hope this is now easier to follow.

L217 phenocrysts or microlites?

R: Microlites, corrected.

L220 label cristobalite with "c" or similar on images.

R: We draw ellipsoid in many cristobalite crystals. In figure 4 cristobalite is now clearly visible on the Si map.

L221 more information on the breccias please. componentry? crystal fragments, or distinct-textured lava/pumice fragments? grainsize? clast morphologies? matrix/clast support?

R: One single pumice fragment was observed when I was doing my master. We have no images available for this and I think that these breccias would deserve a whole separate study. We here just specify that the fragment size is highly variable in line 255.

L226 how big are the clasts? important to know!

R: As said above this information is now provided.

L229 it appears that Fig. 1 goes from panel a to panel p (this is too many for one figure and need to be reduced). Not all are mentioned in the text.

R: We modified and split this figure in 2 as mentioned previously.

Figure 2. Can the vertical texture caption be removed and placed in the figure caption text?

R: Done

L233-234 can we see the bulk rock data subdivided into 1, 2, 3 on Fig. 2, please?

R: Not really because at least half of the clasts analysed for bulk rock were not classified in term of rock type. Anyway, the bulk rock does not show any notable variations between clast types, except for SiO_2 in the type 2 population as mentioned in line 271.

L246 comment on difference between XRD and image analysis numbers - the XRD results suggest far higher crystallinity. why? Also, please provide error bars for crystal proportion estimates.

R: The reasons for discrepancy were explained in lines 300-318, with some additional information in the new version (limits to contrast, size limit using SEM, devitrification…). Here we add some discussion from d'oriano et al 2005 that this contrast issue may be particularly true for trachytes-phonolites for which the glass and feldspar compositions are very close. We now provide error bars for XRD based on a calibration using albite crystals and glass in different proportions and show that the error is less than 5% with this technique, so the discrepancy with image analysis must come from the SEM related issues.

L254 this should be 3b as mentioned later, and lower in the figure.

R: Done

L261 also phases that are indistinguishable from glass in BSE images?

R: Yes. See previous comment

L266-67 why is devitrification an additional cause of discrepancy between crystallinities measured by XRD and image analysis?

R: This was proposed by Rowe et al., 2012. This comes back to the idea that image analysis is limited in size to a certain limit, while XRD can measure crystals down to few nanometer (e.g., that could be formed by devitrification).

L270-271 is that because there is an arbitrary threshold between pumice and dome lava, and a continuum of texture?

R: In fact yes, this is a nice way to show that the transition between the two classes is gradual. However, the clasts classified as pumice really show textural characteristics of

pumice, and the same for the dome rocks. I guess there must be a transitional layer as often proposed for Vulcanian eruptions (i.e. to explain the origin of breadcrust bombs).

L282 do you have Fe-Ti ox analyses showing this?

R: We now add a table in supplementary material with all chemical analysis.

L295 surprising that not more of a compositional spread in the type 3 glasses (as breccias with a range of texture and origin)

R: It would be interesting to study these breccias more in detail in a future study.

L300 comment on range of obtained Tg values and link to quenching rate

R: We now only discuss the signal for the pumice with a clear Tg peak at 690°C because this is the curve with the most reliable signal for quantification of Tg. For the second part of the comment, I am not sure whether the reviewer means the natural quenching rate during or after fragmentation or differences in thermal treatment during the analysis. The thermal treatment was the same for all samples and therefore had no influence on the observed curves. It is true that the natural thermal history of each clast was likely different, but this is hard to evaluate with the present data.

L302 but why the dry viscosity when the measured value of Tg reflects the dissolved water in the glass at the time of quenching, which was presumably non-zero?

R: Now in line 361. We meant that we combine a dry and hydrous viscosity model to estimate the viscosity and water content (of 0.04wt%) at Tg. We also make clear in line 366 that viscosity was likely lower at time of fragmentation if the water content was higher.

L306 could you more clearly explain the rationale for what is being done here? It is something of a circuitous method, and please quantify uncertainties involved (e.g. due to mismatch between PVC and Kilian composition and knock-on effect on the viscosity
L311 how similar and so representative is the PVC composition and so viscosity?

R: We now add more information on this procedure in the supplementary material. Of course, there is some small difference between PVC and Kilian composition, especially the K_2O content that is higher for PVC. We chose the closest trachytic composition to minimize this effect, and most of the oxides are in the range or with differences up to 0.2 wt % compared to Kilian. We note that the Monte Nuovo composition has some elements closer to Kilian but shows on average more differences compared to PVC. Using the same procedure with MNV yields a very similar viscosity at T_g as for PVC, which shows that the composition discrepancies had a limited influence on this analysis.

L313 so, a water content of 0.04 wt % at Tg. Is that similar to the amount of non-degassed water still present in the sample once heated up to 690 C? (e.g. once sub-Tg hydration removed).

R: The mass loss after T_g is negligible as observed in figure 9 (within the error of the measurement). Therefore, this is quite similar to the modelled value of 0.04 wt % that is very low.

The DSC measurement for Tg and TGA measurement were conducted at the same heating rate – were there kinetic degassing effects?

R: There are no degassing effects in the limits of resolution for both T_g and TGA.

L317-320 can you formalise this and quantify sub- and super-Tg mass loss? It looks like ~0.05 wt % at T>690C!

R: We found ~ 150 ppm, which is within the error of the measurement.

L328 there are no viscosity results, but rough estimates of the melt viscosity based up a number of approximations and assumptions.

R: We corrected to viscosity estimation.

L333 glasses within the...

R: Done

L337 we have nothing quantitative about the vesicle deformation, and only a small number of images that we are not sure are representative. the crystallinity data is OK, despite the misfit between XRF and textural outputs, but the degree of deformation does need to be properly characterised.

R: These are just qualitative observations indeed. We now remove statements about vesicle deformation in the discussion as we agree we cannot interpret this so much.

L349 is there no banding between microlite richer- and poorer pumiceous material, as you'd expect to find along the wall of the conduit?

R: We didn’t see this variation in microlite content but this could be. There are clear variations in porosity though, but porosity is lower than 40 vol% in most cases.

L352 could we have an explanation of the degassing model? the magma was erupted at 775 C, and after quenching through Tg contained 0.04 wt % H2O at 690 C. So, what was the likely H2O content at the moment of fragmentation? and was there scope for significant post-fragmentation vesiculation? is there any evidence for that from vesicle textures, e.g. Giachetti papers on SHV bombs, or Saubin 2016?

R: We now specify in lines 366 that we deal with viscosities at time of quenching and that viscosities may have been lower at fragmentation if the water content was higher. We cannot estimate the water content at fragmentation.

There is evidence for post-fragmentation vesiculation with breadcrust bombs. These breadcrust textures are more rare in lapilli and it is therefore hard to tell if there has been significant post-fragmentation expansion in the clasts studied here.

Additionally, breadcrust bombs likely arise from a transitional zone between the dome and the pumiceous conduit, as proposed for SHV and Guagua Pichincha (Giachetti et al., 2010; Wright et al., 2007).

L361 clarify please - in the magma chamber, or conduit?

R: In the conduit. We specify “during magma ascent” now in line 414.

L371-372 do you have any spatial constraints on Cl concentrations, e.g. Cl vs distance from nearest connected vesicle/fracture?

R: Unfortunately no, that would be very interesting though. The problem with such an approach in these trachytes is that the spots of glass are very delicate to find...so an approach like Yoshimura et al is not really feasible here.

L375 are the cracks pre- or post-quench?

R: We cannot really say from the textures.

L396 the colour coding on fig. 3 needs to match the other figures (for type 1, 2, and 3), so that we can easily tell which clasts are being referred to.

R: This was the case (pumice in orange, type 1 in light blue, type 3 in black, the symbols for the XRD beeing the same as in other figures). Type 2 is absent from other figures with glass composition as glass could not be measured with EMPA.

L400 (cristobalite): they need to be labelled in Fig. 1 and mentioned in the Fig. 1 caption.

R: Done (for figure 3)

L418-420 also quantified by Schipper et al 2015 (DOI 10.1007/s00445-015-0925-z), and example of cristobalite textures within context of silicic lava and pore space

R: We discovered this reference recently and agree this is highly relevant. We add it in line 487-494 with some discussion on the two main modes of Silica transport for formation of cristobalite via a vapor source.

L423-424 state why leaching occurs and cite Horwell, Schipper, Damby and others.

R: Agreed. We add a sentence to explain in line 487.

L444 also include Kolzenburg et al 2019 EPSL in this discussion

R: I am not sure what the reviewer was thinking of with including this publication in this specific part.

L449 add Heap et al 2019 as they track porosity-permeability-time paths of sintering tuffisite vein fill: https://doi.org/10.1029/2018JB017035

R: added

L454 rewrite this paragraph. Tuffisite veins are commonly found in bombs ejected during Vulcanian explosions (e.g. Kendrick, Castro 2014, Saubin, etc...). Mention that there is also strong evidence (Saubin) for multiple, repeated fragmentation events - this nicely fits with your story.

R: We rewrote to add Saubin reference about repeated fragmentation events and about Vulcanian activity at Chaitén (lines 527-532)

L466-67 how about loss of volatile Na and K via diffusion from fine-grained matrix of brecciated type 3 clasts?

R: This is interesting. But that does not solve the problem for the other elements.

L469 we need to review the big picture here - are we talking about explosive-effusive transitions at Kilian, or about Vulcanian explosions?

R: First sentence related to Kilian. We now specify this in line 544.

L478-79 I'd argue that, on a small scale at least, Saubin et al 2016 show that this was not the case for Chaitén - there were repeated conduit re-invasions prior to the final bomb ejection in a Vulcanian blast. similar models are proposed by Paisley 2019 volcanica and others.

R: We agree with the reviewer but this is a matter of time and space indeed.

Here we depict the broad picture of conduit replenishment rather than the small scale processes that can occur for instance in tuffisite veins such as ash venting. This small scale process likely occurs at Kilian as discussed elsewhere in the manuscript.

Arguments for a single batch replenishment of the conduit can be the fast ascent rate and crystallization causing rapid emplacement and stalling at the top of the conduit and the gradual textural variation between pumice and dome rocks with textural differences reflecting a vertical variation in decompression, cooling and degassing.

Additionally, we note that the case of Kilian is likely closer to Vulcanian episodes occurring in crystal-rich andesitic to dacitic magmas (e.g., SHV, Guagua Pichincha) than for a rhyolitic crystal poor case such as Chaitén or Cordon Caulle.

L485 resided deeper in the conduit at the time of Vulcanian excavation

R: Done

L500 it must be a matter of scale - the outer crust of the dome will have been glassier, but it might have been so thin it was not represented in your choice of samples.

R: We agree with the reviewer that this may be a possibility. However, the crystallinity would still be quite high likely despite of faster quenching due to previous crystallization by decompression and degassing.

L508 what is the evidence for more than one phase? do the data presented here relate to a sampled stratigraphy that proves there were repeated Vulcanian events? if so, would be great to mention this!

R: We mention this earlier in line 226 and refer to Colombier et al 2017.

L511 sintering does not promote outgassing. remove this reference - papers by Wadsworth, Farquharson, Heap and others are more useful here.

R: It does not promote, but outgassing can occur during sintering as long as we have a connected network. And since this occurs down to very low percolation thresholds (phi ~ 0.04 to 0.09 depending on crystal content) outgassing is not impeded during most of the

sintering process. We rephrased to say it is promoted “by intergranular connected pore space in tuffisite veins” and took the Heap et al 2019 ref.

L513-514 out of interest -what is your explanation for there being no cristobalite precipitation in the dome interior? Is it because it is the source of the stripped SiO2? if so, state this somewhere!

R: This is what we discuss in lines 480-487, that we may have leaching from the SiO2 from the dome interior, and that this SiO2 is then transported to the exterior explaining the excess bulk SiO2 in the Type 2 rocks. We also add explanations in lines 487-494.

L544 magma does not have to fragment at Tg. instead, the vesicular magma most likely quenched through Tg *after* fragmentation. otherwise there would be no post-fragmentation vesiculation. is there any independent evidence for cooling of the magma prior to fragmentation, such as the PT conditions for the crystallised microlite/microphenocryst phases? if not, i'd like to see a discussion of plausible fragmentation temperatures ranging from Tmag = 775 down towards Tg at 690.

R: We agree with the reviewer. We corrected to “at the time of quenching” in line 621.

L546 water can be far better inferred from the TGA by measuring mass loss at high T. see earlier comments, and also more formal treatment by Giachetti, Bindeman and others.

R: See our previous reply on this aspect.

L552-554 absolutely. could we have a rough estimate of this viscosity boost, even just via the Einstein-Roscoe equation?

R: This is a very interesting comment and we thought about it. However, I believe estimating the maximum packing of these systems with polydisperse CSD and a broad range of aspect ratio is very difficult. I think this will be interesting to investigate this more in detail in the future following previous experimental works (e.g., Mueller et al 2011; Klein et al., 2018). Very likely we are above the maximum packing in the dome rocks which would bring the system close to Tg with a system that cannot flow anymore (dome carapace). I think this is very interesting but beyond the scope of this manuscript.

L557-559 although it needs to be recognised that, in some cases, the preserved petrological evidence indicates broadly similar ascent rates for explosive and effusive rhyolitic magma. the ascent rate in the top tens/hundreds of metres may differ but this may not be recorded in the textures.

R: This is based on the compilation given by Cassidy et al., 2018

L564 please define what shallow depth refers to.

R: Done

L565 comments on Figure 8: This looks like it could be a very nice compilation, but what is the y axis? depth = final pressure that the experiments were decompressed to? assuming what pressure gradient? magmastatic or lithostatic? please explain.

R: We used the magmastatic pressure gradient initially. We modify this in the current version and use the standard lithostatic value of 2600 Kg.m-3.

There is also a large spread of crystallinity at any given depth, especially for the slow decompression experiments. the diffusivity of andesite and rhyolite are significantly different, so could you subdivide both fast and slow experiments into these different compositions?

R: We do this separation in the supplementary figure SM1 and show that trachytes crystallize extensively even at much higher decompression rate.

Finally, ideally we'd see the crystallinity as a function of decompression rate as well, as simply faster/slower than 3.6 MPa/h-1 is a very crude separation. what happens if you plot crystallinity vs decompression rate over a small number of binned depths (e.g. 0-2 km, 2-4, 4-6, 6-8)? This would reveal a lot more about links between attained crystallinity and decompression rate.

R: See the previous reply. We did not do the binned depth but we see from figure 11 that the high crystallinity data for both trachytes and subalkaline compositions occur at ~0-2 km. And we see in that the decompression rate is higher for trachytes in this case.

L567 compilation in Fig. 9: this is interesting. suggest rename Vulcanian and Plinian eruptions as pyroclasts: Vulcanian and Plinian, are you're talking about the product, not the process.

R: We mention in the caption that we speak about volcanic rocks associated to these eruptive styles. We kept the figure (and the new legend) as it is for simplicity.

L567: “We also find that the range of experimental crystallinities at fast and slow decompression rates match the microlite contents of explosive and effusive andesitic and rhyolitic natural rocks, respectively (Fig. 8; Fig. 9).”

What is being said here, and is it meaningful? Fig. 8 shows a huge range of crystallinities attained (as a large compositional range from andesite to rhyolite and a

broad range of decompression rates within both the “slow” and the “fast” categories). Essentially, the experimental range is 0% to ~100 % crystallinity, and the “natural” range is 0 to ~90 %. What can be drawn from this?

R: We rephrased in lines 646-655.

Yes, both plots are wedge-shaped, as Fig. 8 plots crystallinity against depth, and Fig. 9 against porosity – is this the point, that porosity and depth are reflecting the same decompression story? It’s not a simple story, though, as there can be diverse initial volatile concentrations and homogeneous/heterogeneous vesicle nucleation.

R: This is not the point that is made here and these two figures are distinct. We now make clear for the previous comment that we compare the range of microlite content near the surface for experimental and natural data.

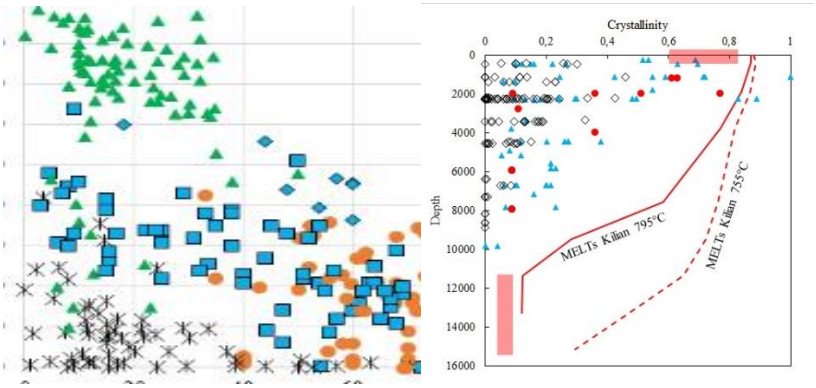

L569 rewrite this. simply, that the crystallinity in fast-decompressed trachyte is higher than fast-decompressed andesite and rhyolite. I'd be particularly keen to see crystallinity attained vs decompression rate for trachtye vs separated andesite and rhyolite!

R: Done

L571-573 this is a great sentence and is much more clearly expressed!

R: Thanks :)

L577-578 there is such a large range of experimental decompression rate that we do need to see crystallinity vs actual decompression rate value – the range of experimentally attained crystallinity is ~0 to ~100%

R: Done

L591 implicit within this is that the crystals cannot move independently of the host melt. however we are talking about initial melt viscosities that are exceptionally low (10^1-10^2 Pa.s). which phases are crystallising, what is their density contrast with the melt, and is there scope for significant Stokes settling during a plausible range of magma ascent rates?

What does the evolution of melt composition and bulk composition in your variably crystalline samples - Fig. 4 - tell you about the mobility of in-situ grown crystals? are they being separated from the melt, or not?

R: See our previous reply on this topic.

L597 again, need to consider scope for magma-melt separation, especially in lower viscosity, higher H2O magma at depth. sure, as the magma stiffens the crystals will be "locked in" any effectively immobile, but what about these intermediate depths of 3-8 km?

R: See previous reply

L621 this is good. more scope for positive feedback, especially once crystallisation kicks in and greatly increases magma viscosity.

L640 only if significant outgassing is possible, otherwise diffusivities will be high and some crystal growth will be expected, even at modest undercoolings.

R: That is specified in the second part of the sentence.

L644 this is very interesting and takes into slug dynamics within shallow magma - so the viscosity is low enough to permit gas slug ascent. i do think discussion of stokes law for both crystals and bubbles, in general for trachytic conduits, is an useful thing to add here.

R: See previous reply to main comment about Stokes.

L649 this section is very nicely argued and consistent with what has been presented.

Figures – some comments on the .pdf

R: We will reply to these comments in this document

L1015 would be good to add a key on the graph itself so the reader can easily see which data is which. Add a section panel of crystallinity vs decompression rate for binned final depths (0-2, 2-4 km, etc...)

R: We now add legends in most figures

Figure 7: redraw - the tuffisite vein is unrealistically wide!

but...you think that type 3 is ONLY from discrete tuffisite veins, as opposed to a broader zone of fragmented and reannealed magma?

R: Now figure 10. Agreed for the scale!! We made them smaller, however we mention that they are still unrealistically wide in the caption but that this is just for illustration. We cannot really know how they are localized in the conduit so we keep a simple illustration here for this conceptual model.

Figure 8: what if deep-formed crystals separated out of magma due to density difference? could calculate stokes settling velocity for appropriate size and composition phenocryst as magma goes through degassing path. it will become immobile on reasonable timeframes, but where in the system? does this relate to the compostional evolution of the magma?

R: See previous replies on this topic

Tables: BV might want you to replace 0,7 commas with 0.7 points (sorry for imposing British conventions, I am fine with either!)

R: Corrected

Best wishes, Hugh Tuffen

Figure 1

Click here to access/download;Figure;Figure 1-NEW.jpg

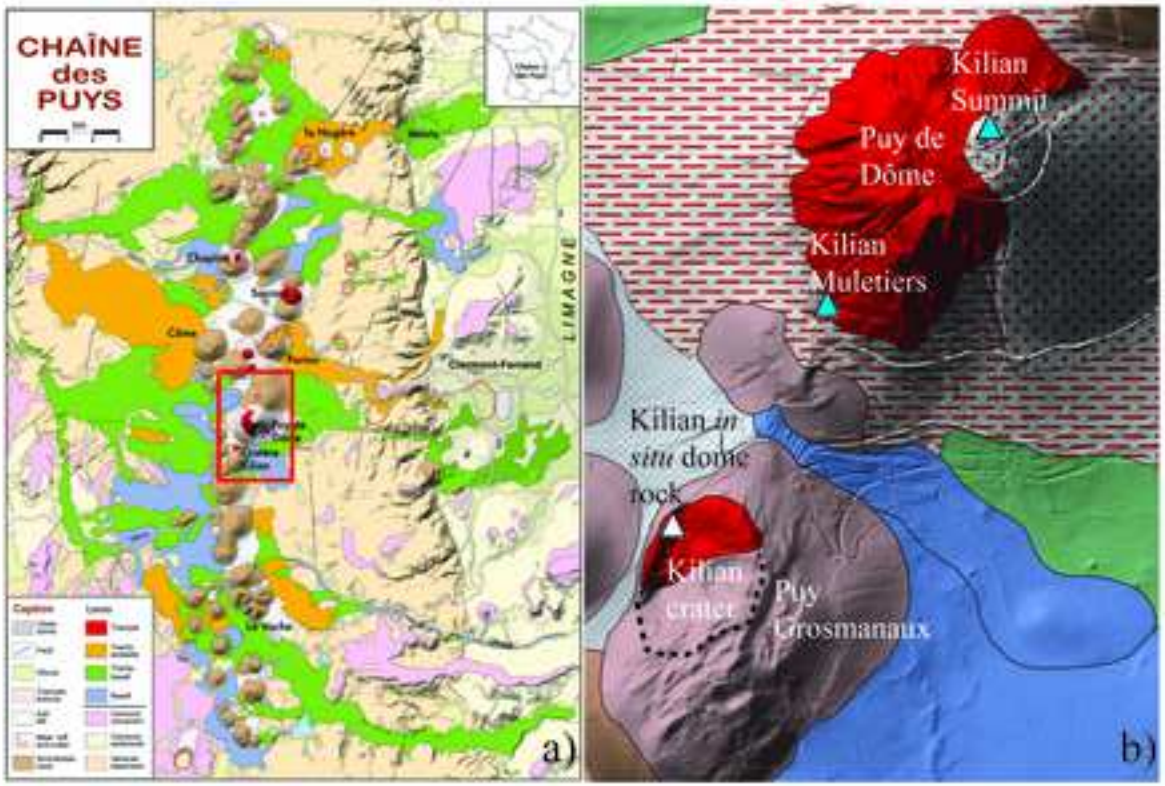

Figure 2

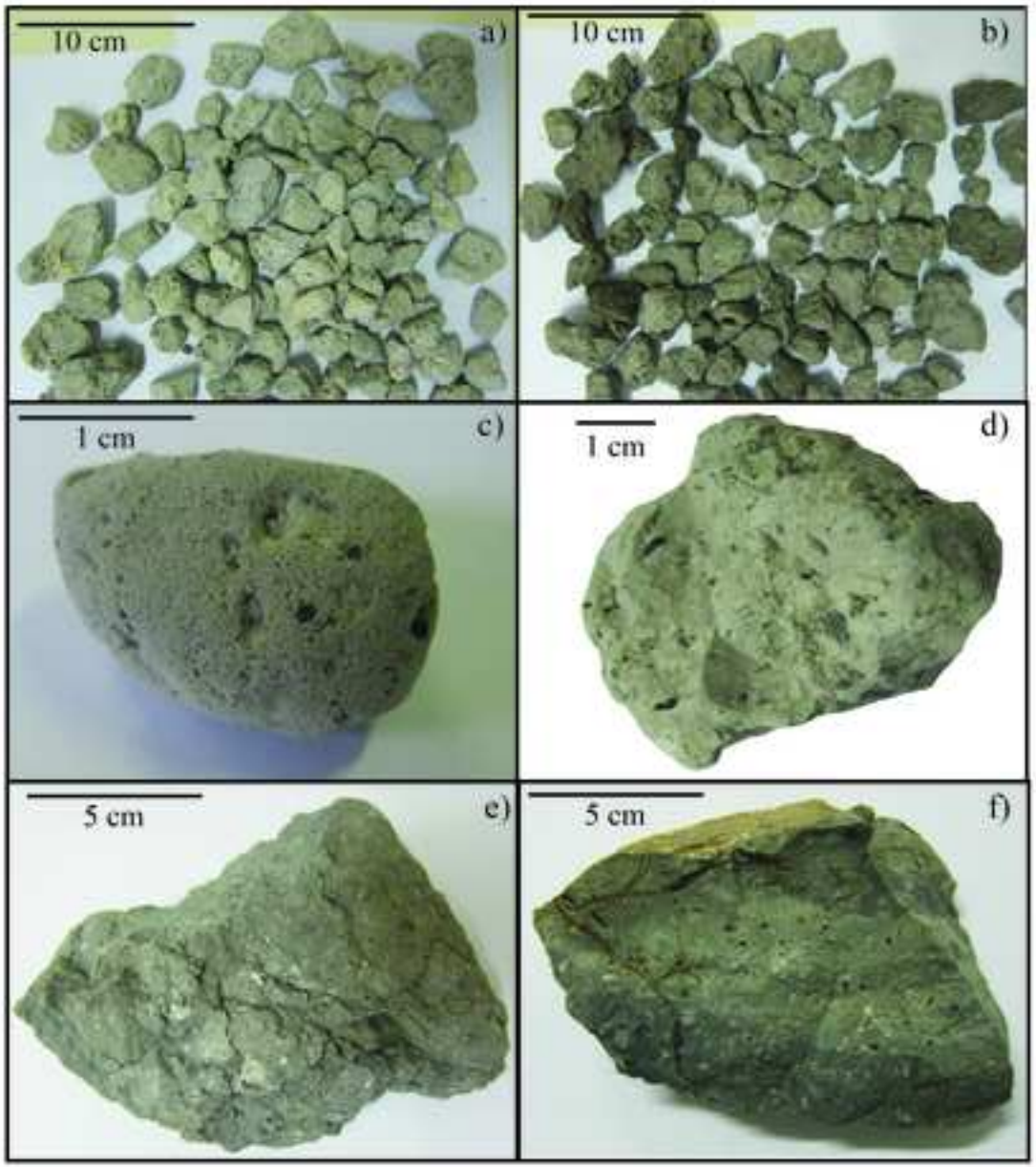

Figure 3

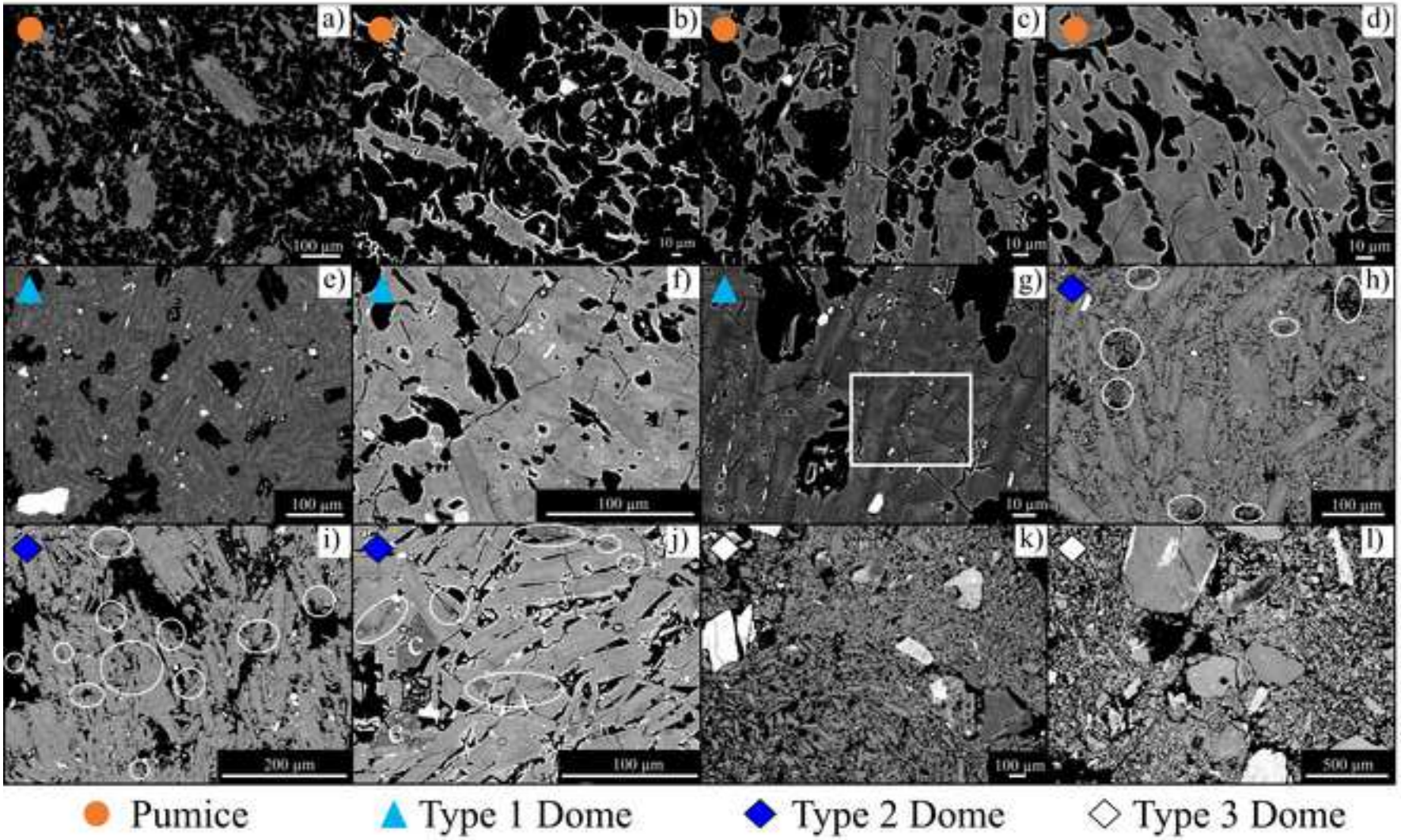

Figure 4

Click here to access/download;Figure;Figure 4-NEW.jpg

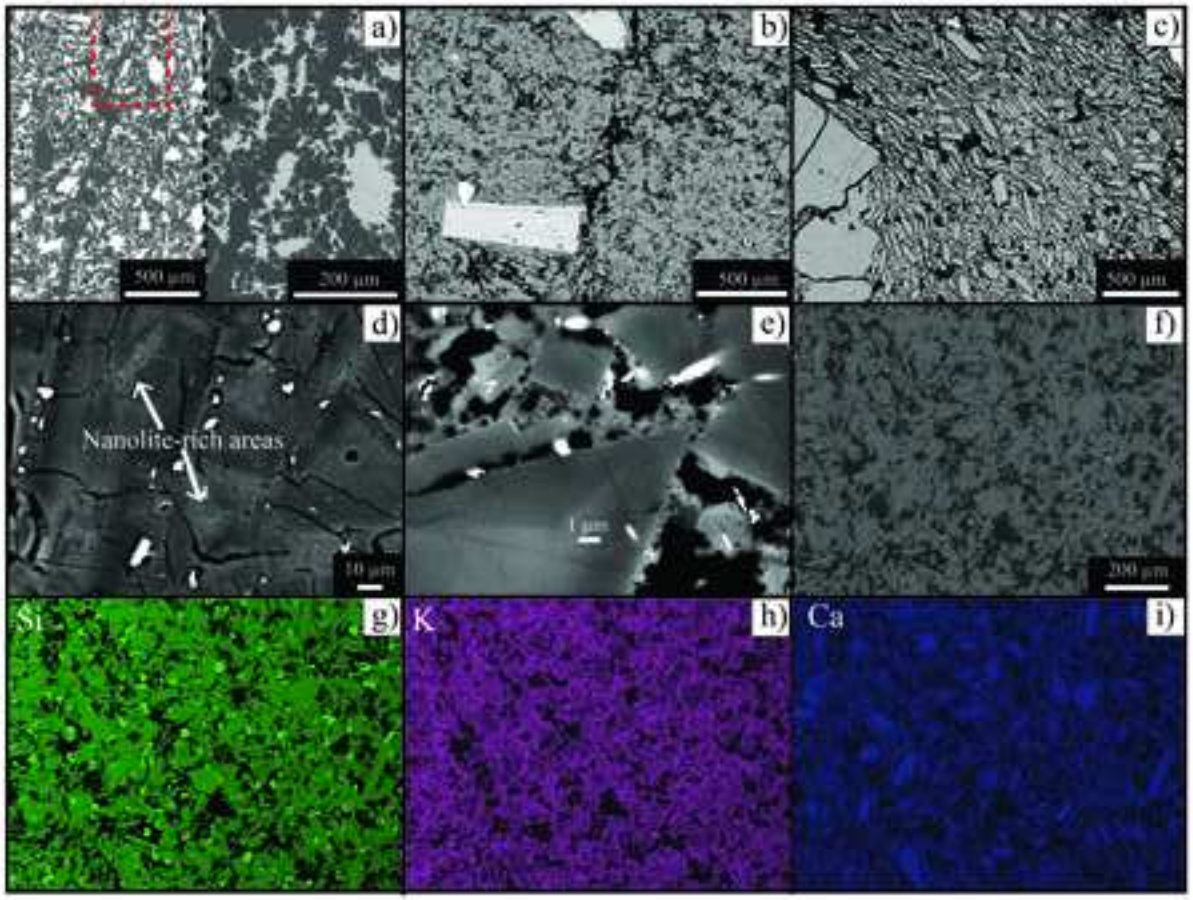

Figure 5

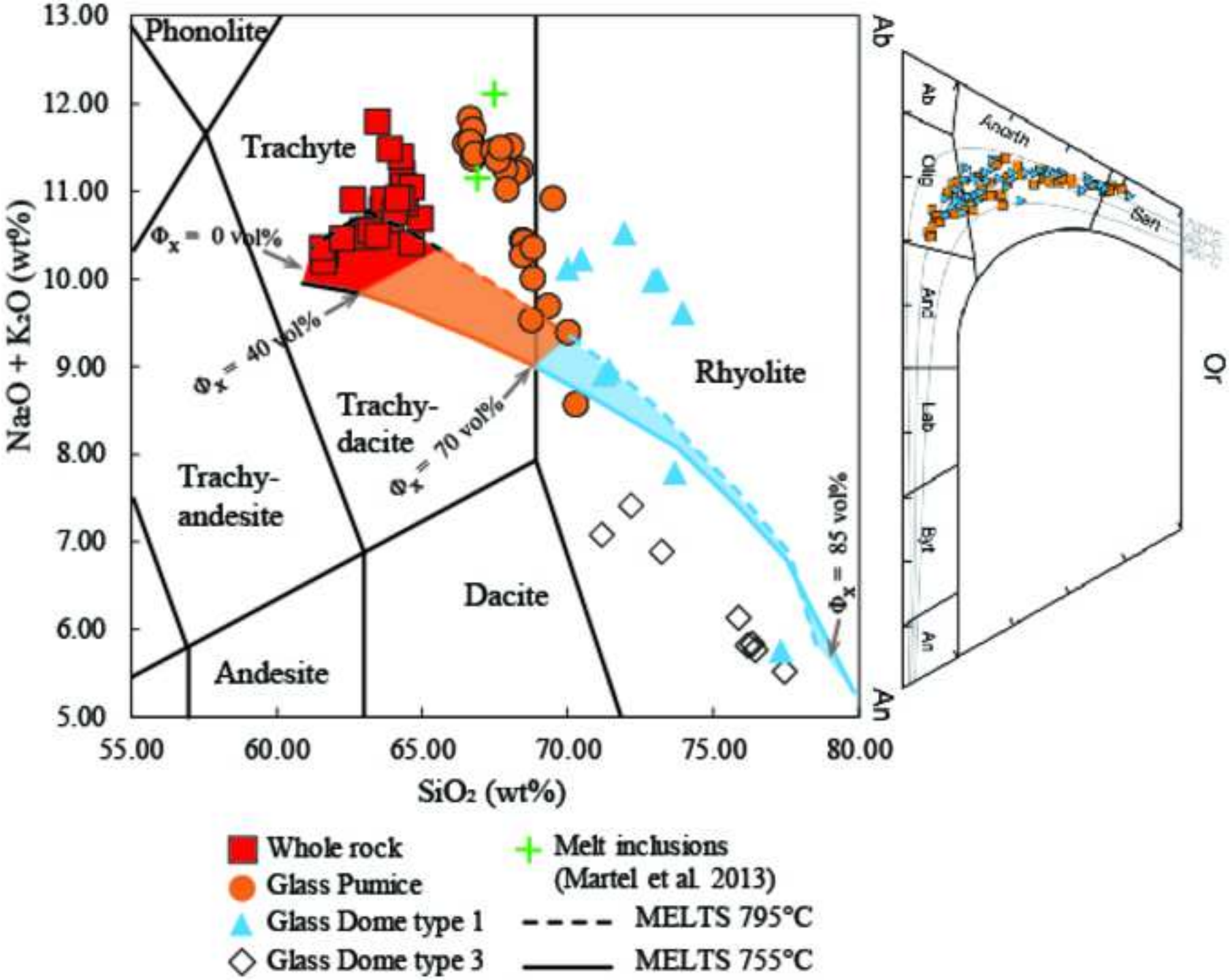

Figure 6

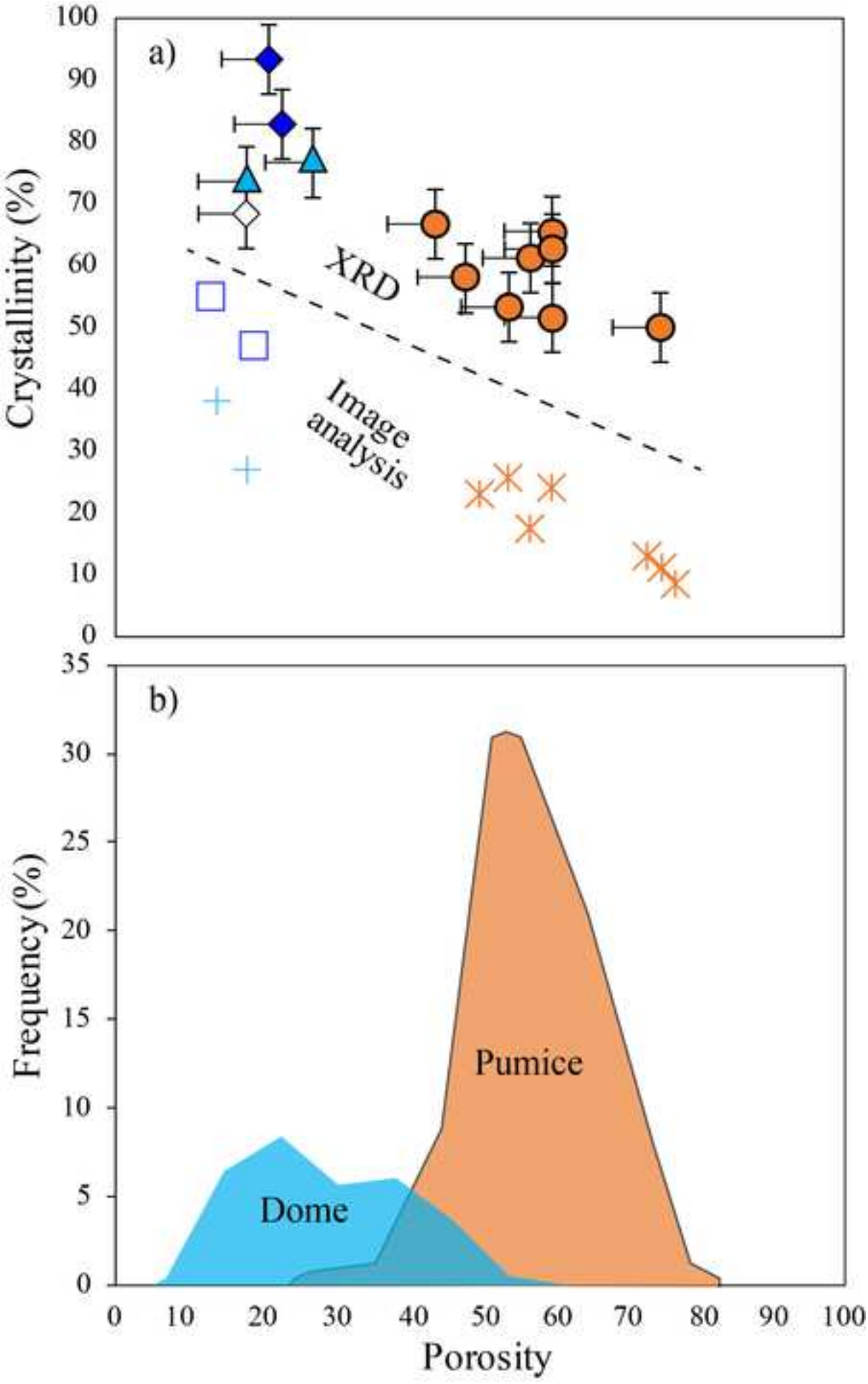

Figure 7

Click here to access/download;Figure;Figure 7-NEW.jpg

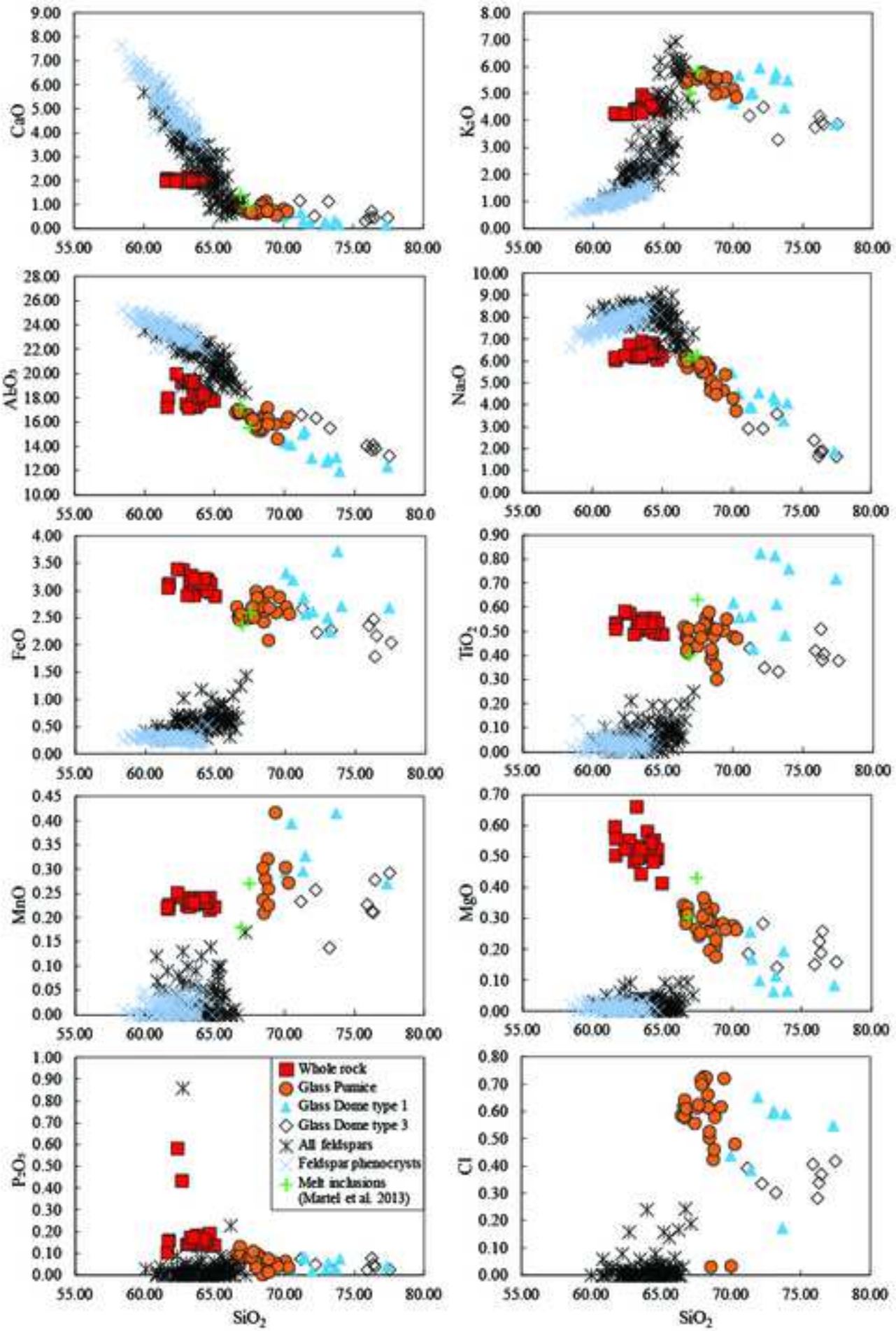

Figure 8

Click here to access/download;Figure;Figure 8-NEW.jpg

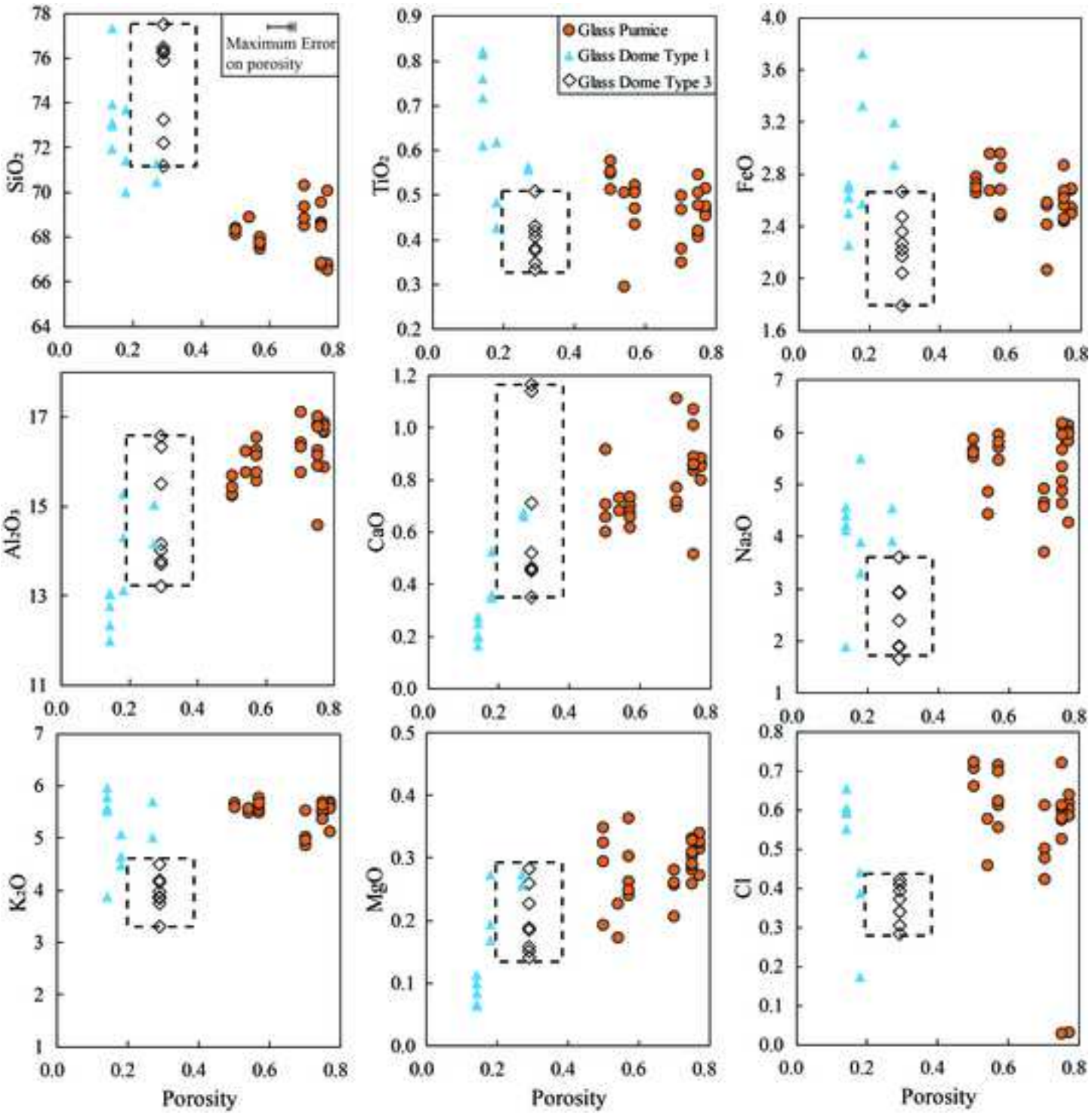

Figure 9

Click here to access/download;Figure;Figure 9-NEW.jpg

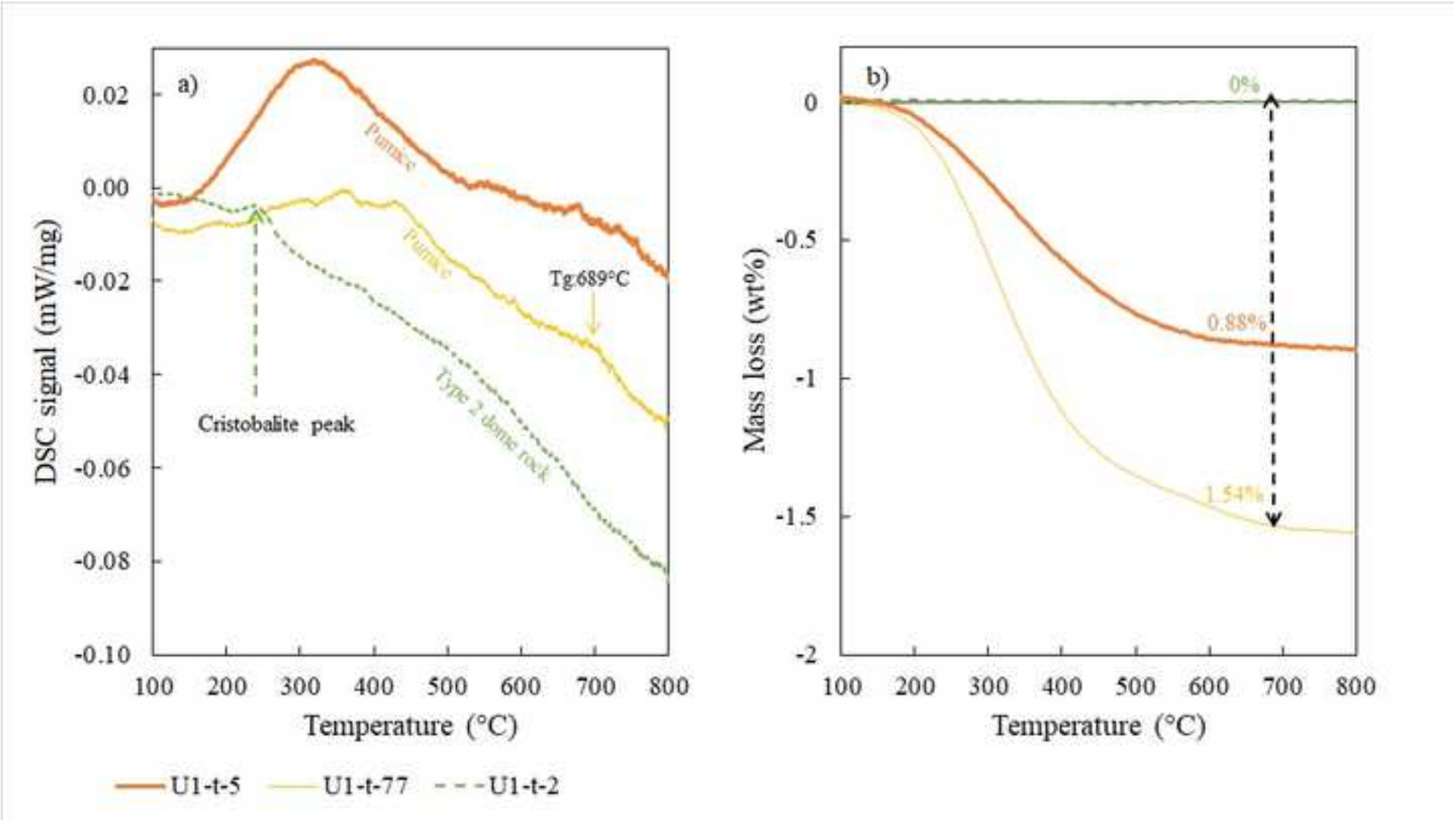

Figure 10

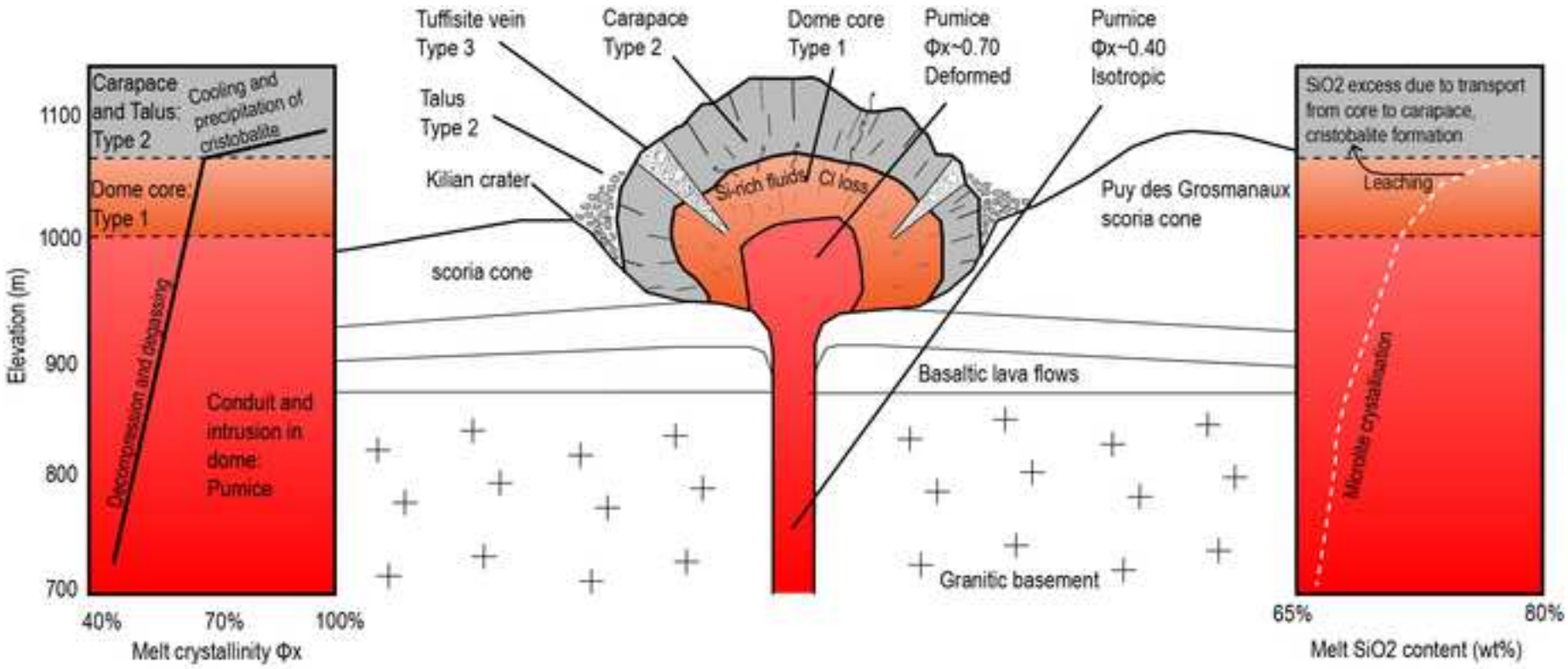

Figure 11

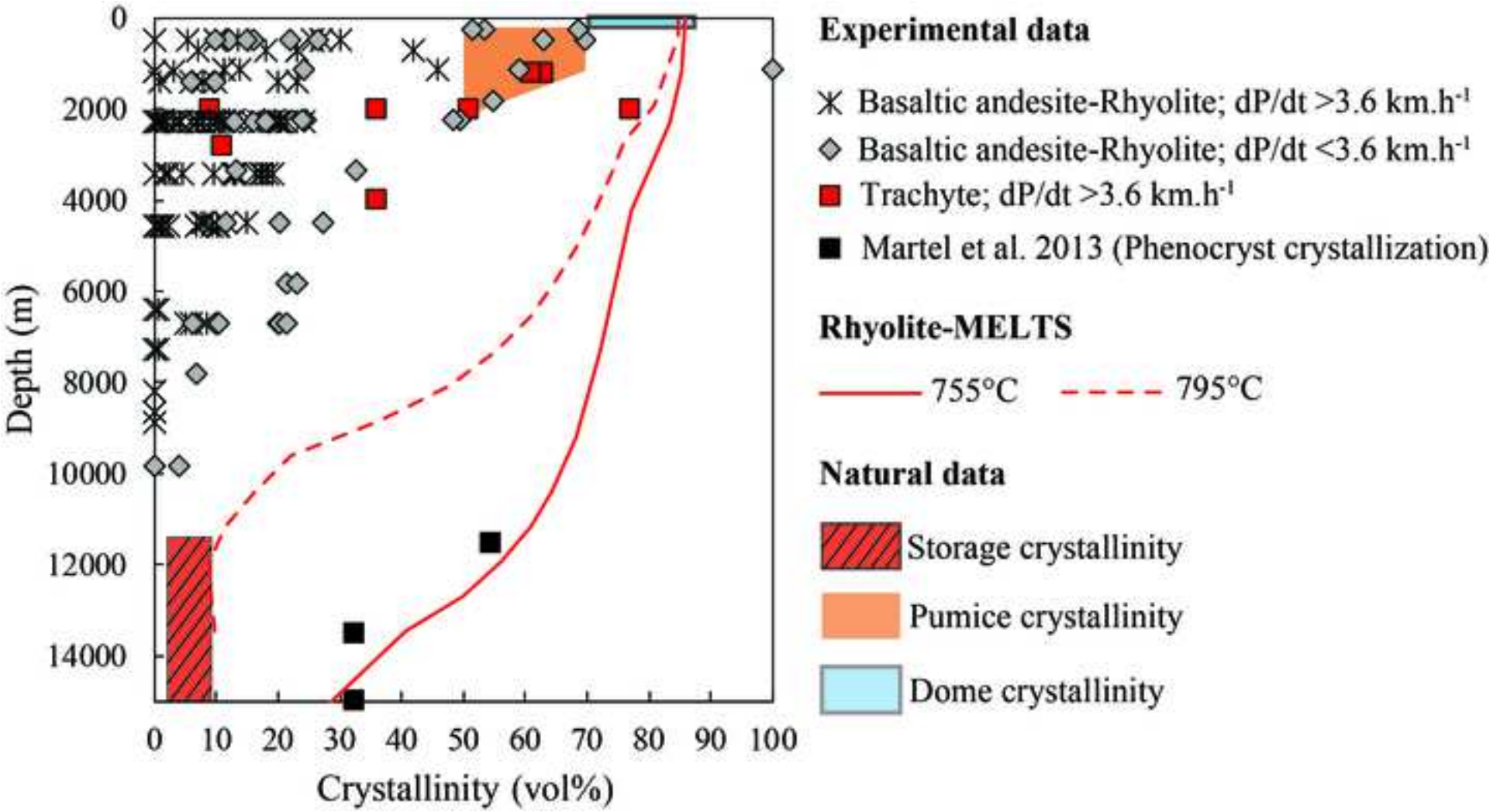

Figure 12

Click here to access/download;Figure;Figure 12-NEW.jpg

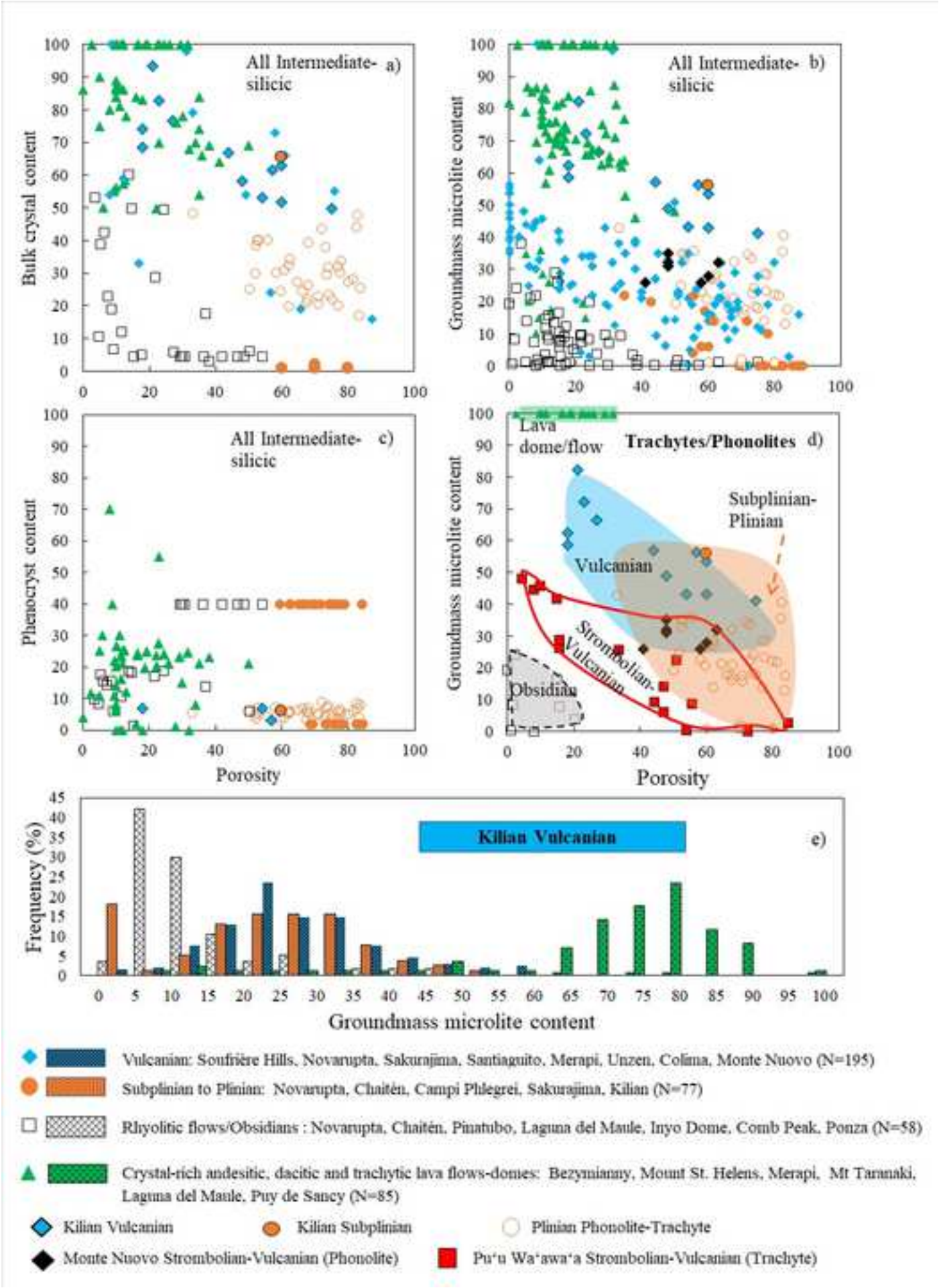

Table 1

Sample	Sample type		Grain size fraction (mm)
K2_1	Pumice; Pyroclast		16-32
K1_s_1			16-32
U1-t-77			16-32
U1_b_28			16-32
K1_t_1			16-32
U1_b_63			32-64
K1_t_63			16-32
U2_b_29*			32-64
U1_t_3			32-64
K2 Mul 2			16-32
U1_b_71			16-32
K1_b_61	Dome rocks; Pyroclast	Type 1	16-32
K1_s_2			16-32
K2 Mul 3			16-32
K2 Mul 4			16-32
U1_b_97			16-32
PB11-1803-2b1			-
K2 Mul 5		Type 2	16-32
U1_t_6			32-64
K1_t_64			16-32
U1_b_96			16-32
U1-t-2			-
K1_b_4			16-32
K1-s-3			-
K2_s_2		Type 3	16-32
U1_t_4			16-32
PB11-1803-2a			-
PB11-1803-2c			-
K2_s_3			16-32
U1_b_81			-
BPK-1	In situ Type 2 dome rock; sampled at the exterior of the dome		-

* clast from Sub-Plinian activity

Porosity[a]	Permeability[a]	Crystallinity SEM[a] (vol %)	Crystallinity XRD (vol %)	Presence of cristobalite	EPMA glass
0.6	-	-	45.4	-	-
0.6	-	-	54.4	-	-
0.75	-	11	40.4	-	Yes
0.77	-	8.5	-	-	Yes
0.73	7.7E-13	13	-	-	Yes
0.57	2.5E-12	17.5	49.9	-	Yes
0.54	1.5E-13	25.5	46.7	-	-
0.6	2.7E-12	23.9	51.6	-	-
0.44	6.2E-13	-	65.2	-	-
0.48	-	-	53.2	-	-
0.5	1.3E-12	23	-	-	Yes
0.18	-	27	66.7	-	Yes
0.27	-	-	69.1	Yes	Yes
0.39	3E-12	-	-	-	-
0.39	1.4E-12	-	-	-	-
0.14	-	38	-	-	Yes
-	-	-	-	-	-
0.21	6.6E-13	-	83.9	Yes	-
0.23	1.6E-12	-	89.1	Yes	-
0.13	2.7E-15	55	-	Yes	-
0.19	-	47	-	Yes	-
0.2	3.90E-16	-	-	Yes	-
0.21	-	-	-	Yes Yes	-
0.27	-	-	-	-	-
0.27	1.4E-13	-	59.51	-	Yes
-	-	-	-	Yes	Yes
-	-	-	-	Yes	Yes
0.19	-	-	-	-	-
-	-	-	-	-	-
-	-	-	-	Yes	-

XRF	Textural observations
Yes	-
-	-
Yes	Yes
-	Yes
-	Yes
Yes	Yes
-	Yes
Yes	Yes
Yes	-
-	-
-	Yes
-	Yes
Yes	-
-	Yes
-	Yes
-	Yes
-	-
Yes	Yes
Yes	Yes
-	Yes
-	Yes
-	Yes
-	Yes
	Yes
-	Yes
Yes	Yes
-	Yes
-	Yes
-	Yes
-	Yes
-	Yes; Chemical mapping

Table 2

Sample	Sample type	Porosity	Crystallinity	Proportion of phases (v		
				Anorthoclase	Oligoclase	Kaersutite
K1_t_63	Pumice	0.54	53.2	26.8	26.3	-
U2_b_29	Pumice	0.6	65.5	36.3	29.3	-
U1_b_63	Pumice	0.57	61.5	23.6	37.9	-
U1_t_3	Pumice	0.44	66.7	37.1	29.6	-
U1_t_77	Pumice	0.75	49.9	26.0	24.0	-
K1_s_1	Pumice	0.6	62.9	27.5	35.4	-
K2 Mul 2	Pumice	0.48	58.1	25.3	32.8	-
K2_1	Pumice	0.6	51.8	14.9	36.9	-
K1_b_61	Dome Type 1	0.18	74.0	35.3	36.4	2.2
K1_s_2	Dome Type 1	0.27	76.7	32.8	40.0	-
K2 Mul 5	Dome Type 2	0.21	93.5	67.9	19.1	-
U1_t_6	Dome Type 2	0.23	82.9	24.7	51.9	-
U1_t_4	Dome Type 3	0.18	68.4	31.5	36.9	-

ol %)

Cristobalite	Glass	χ^2
-	46.8	1.21
-	34.5	1.27
-	38.5	1.32
-	33.3	1.1
-	50.1	1.04
-	37.1	1.2
-	41.9	1.31
-	48.2	1.17
-	26.0	1.4
3.9	23.3	2.21
6.5	6.5	1.5
6.3	17.1	1.92
-	31.6	3.54